Inputs and processes affecting the distribution of particulate iron in the North Atlantic along the GEOVIDE (GEOTRACES GA01) section

Arthur Gourain[1,2], Hélène Planquette[1], Marie Cheize[1,3], Nolwenn Lemaitre[1,4], Jan-Lukas Menzel Barraqueta[5, 6], Rachel Shelley[1, 7], Pascale Lherminier[8] and Géraldine Sarthou[1]

1-UMR 6539/LEMAR/IUEM, CNRS, UBO, IRD, Ifremer, Technopôle Brest Iroise, Place Nicolas Copernic, 29280 Plouzané, France

2- now at Ocean Sciences Department, School of Environmental Sciences, University of Liverpool, Liverpool, L69 3GP, United Kingdom

3- now at Ifremer, Centre de Brest, Géosciences Marines, Laboratoire des Cycles Géochimiques (LCG), 29280 Plouzané, France

4- now at Department of Earth Sciences, Institute of Geochemistry and Petrology, ETH-Zürich, Zürich, Switzerland

5- GEOMAR, Helmholtz Centre for Ocean Research Kiel, Wischhofstraße 1-3, 24148 Kiel, Germany

6- now at Department of Earth Sciences, Stellenbosch University, Stellenbosch, 7600, South Africa

7- now at Earth, Ocean and Atmospheric Science, Florida State University, Tallahassee, Florida, 32310, USA

8- Ifremer, Univ. Brest, CNRS, IRD, Laboratoire d'Océanographie Physique et Spatiale (LOPS), IUEM, F-29280, Plouzané, France

Correspondence to: helene.planquette@univ-brest.fr

Abstract

The aim of the GEOVIDE cruise (May-June 2014, R/V *Pourquoi Pas?*) was to provide a better understanding of trace metal biogeochemical cycles in the North Atlantic Ocean. As marine particles play a key role in the global biogeochemical cycle of trace elements in the ocean, we discuss the distribution of particulate iron (PFe), in relation to the distribution of particulate aluminium (PAl), manganese (PMn) and phosphorus (PP). Overall, 32 full vertical profiles were collected for trace metal analyses, representing more than 500 samples. This resolution provides a solid basis for assessing concentration distributions, elemental ratios, size-fractionation, and adsorptive scavenging processes in key areas of the thermohaline overturning circulation. Total particulate iron concentrations ranged from as low as 9 pmol L^{-1} in surface waters of the Labrador Sea to 304 nmol L^{-1} near the Iberian margin, while median PFe concentrations of 1.15 nmol L^{-1} were measured over the sub-euphotic ocean interior.

Within the Iberian Abyssal Plain, the ratio of PFe to PAl was identical to the continental crust molar ratio (0.21 mol mol^{-1}), indicating the important influence of crustal particles in the water column. Overall, the lithogenic

component explained more than 87% of PFe variance along the section. Within the Irminger and Labrador basins, the formation of biogenic particles led to an increase of the PFe/PAl ratio (up to 0.64 mol mol^{-1}) compared to the continental crust ratio. Continental margins provide high quantities of particulate trace elements (up to 10 nmol L^{-1} of PFe) to the open ocean. For example, horizontal advection of PFe was visible more than 250 km away from the Iberian margin. Additionally, several benthic nepheloid layers were observed more than 200 m above the seafloor along the transect, especially in the Icelandic, Irminger and Labrador basins, suspending particles with high PFe content of up to 89 nmol L^{-1}.

1. Introduction

Particles play a key role in the ocean where they drive the residence time of most elements (Jeandel and Oelkers, 2015), and strongly influence the global biogeochemistry of macro- and micro-nutrients including iron (Milne et al., 2017). In the surface ocean, biological activity produces biogenic suspended matter through planktonic organisms, while atmospheric deposition (Baker et al., 2013; Jickells et al., 2005), riverine discharge (Aguilar-Islas et al., 2013; Berger et al., 2008; Ussher et al., 2004) or ice-melting (Hawkings et al., 2014; Lannuzel et al., 2011, 2014) deliver mostly lithogenic derived particles to surface waters. These particulate inputs are highly variable, both spatially and seasonally, in the world's oceans. At depth, benthic and shelf sediment resuspension (e.g. Aguilar-Islas et al., 2013; Cullen et al., 2009; Elrod et al., 2004; Fitzwater et al., 2000; Hwang et al., 2010; Lam et al., 2015; Lam and Bishop, 2008; McCave and Hall, 2002), and hydrothermal activity (Elderfield and Schultz, 1996; Lam et al., 2012; Tagliabue et al., 2010, 2017; Trefry et al., 1985), provides important amounts of particles to the water column. Moreover, authigenic particles can be produced *in-situ* by aggregation of colloids (Bergquist et al., 2007) or oxidation processes (Bishop and Fleisher, 1987; Collier and Edmond, 1984). Thus, oceanic particles result from a complex combination of these different sources and processes (Lam et al., 2015).

In the upper water column, the total iron pool is dominated by marine particles (Radic et al., 2011) which strongly interact with the dissolved pool (e.g. Ellwood et al., 2014). Indeed, dissolved iron can be scavenged onto particles (Gerringa et al., 2015; Rijkenberg et al., 2014), incorporated into biogenic particles (Berger et al., 2008) or produced by remineralisation of particles (Dehairs et al., 2008; Sarthou et al., 2008). Interestingly, the concept of "reversible scavenging" (i.e. release at depth of dissolved iron previously scavenged onto particles) has been advocated recently (Dutay et al., 2015; Jeandel and Oelkers, 2015; Labatut et al., 2014), while other studies reveal distinct dissolution processes of inorganic particulate iron (e.g. Oelkers et al., 2012; Cheize et al., 2018). Slow dissolution of particulate iron at margins has also been evoked as a continuous fertilizer of primary production and should be considered as a source of dissolved iron (e.g. Jeandel et al., 2011; Jeandel and Oelkers, 2015; Lam and Bishop, 2008). Within or below the mixed layer, the rates of regeneration processes can also impact the bioavailable pool of iron, among other trace metals (e.g. Ellwood et al., 2014; Nuester et al., 2014). However, the rates of these processes are not yet fully constrained. The study of particulate iron is thus essential to better constrain its marine biogeochemical cycle. Interest has grown in this subject over the last 10 years, in particular (e.g. Bishop and Biscaye, 1982; Collier and Edmond, 1984; Frew et al., 2006; Lam et al., 2012; Milne et al., 2017; Planquette et al., 2011, 2013; Sherrell et al., 1998) and, to our knowledge, only two studies have been performed on an ocean-wide scale: the GA03 GEOTRACES North Atlantic Zonal Transect (Lam et al., 2015; Ohnemus and Lam, 2015) and the GP16 GEOTRACES Pacific Transect (Lam et al., 2017; Lee et al., 2017).

Within this global context, this paper presents the particulate iron distribution of the North Atlantic Ocean, along the GEOTRACES GA01 section (GEOVIDE), and discusses the various sources and processes affecting particulate iron (PFe) distribution, using particulate aluminium (PAl), phosphorus (PP) or manganese (PMn) distibutions to support our conclusions.

2. Methods

2.1. Study area

Particulate samples were collected at 32 stations during the GEOVIDE (GEOTRACES GA01 section) cruise between May and June 2014 aboard the R/V *Pourquoi Pas?* in the North Atlantic Ocean (Sarthou et al., 2018). The sampling spanned several biogeochemical provinces (Figure 1), starting over the Iberian margin (IM, Stations 2, 4 and 1), and proceding to the Iberian Abyssal Plain (IAP, Stations 11 to 17), the Western European Basin (WEB, Station 19 to Station 29) and the Icelandic Basin (IcB, Stations 32 to 36). Then, samples were collected above the Reykjanes Ridge (RR, Station 38), in the Irminger Basin (IrB, Stations 40 to 60), close to the Greenland shelf (GS, Stations 53, 56 and 61), the Labrador Basin (LB, Stations 63 to 77) and finally close the Newfoundland shelf (NS, Station 78) (Figure 1). The North Atlantic is characterized by a complex circulation (briefly described in section 3.1 and in detail by Zunino et al. (2017) and García-Ibáñez et al. (2015)) and is one of the most productive regions of the global ocean (Martin et al., 1993; Sanders et al., 2014).

2.2. Sampling

Samples were collected using the French GEOTRACES clean rosette, equipped with twenty-two 12 L GO-FLO bottles (two bottles were leaking and were not deployed during the cruise). GO-FLO bottles (General Oceanic's) were initially cleaned in the home laboratory (LEMAR) following the GEOTRACES procedures (Cutter and Bruland, 2012). The rosette was deployed on a 14 mm Kevlar cable with a dedicated, custom-designed clean winch. Immediately after recovery, the GO-FLO bottles were individually covered at each end with plastic bags to minimize contamination. Bottles were then transferred into a clean container (class-100) for sampling. On each cast, nutrient and/or salinity samples were taken to check potential leakage of the GO-FLO bottles.

Filters were cleaned following the GEOTRACES protocols (http://www.geotraces.org/images/Cookbook.pdf) and kept in acid-cleaned 1 L LDPE bottles (Nalgene) filled with ultrapure water (Milli-Q, resistivity of 18.2 MΩ cm) until use. All filters were 25 mm diameter in order to optimize the signal over the filter blank, except at the surface depth where 47 mm diameter filters were used. The filters were mounted on acid-cleaned polysulfone filter holders (Nalgene™). Prior to filtration, the GO-FLO bottles were shaken three times, as recommended in the GEOTRACES cookbook to avoid settling of particles in the lower part of the bottle. GO-FLO bottles were pressurized to < 8 psi with 0.2 µm filtered nitrogen gas (N_2, Air Liquide). Seawater was then filtered directly through paired filters (Pall Gelman Supor™ 0.45 µm polyetersulfone, and Millipore mixed ester cellulose MF 5 µm) mounted in Swinnex polypropylene filter holders (Millipore), following Planquette and Sherrell (2012) inside the clean container. Filtration was operated until the bottle was empty or until the filter clogged; the volume filtered ranged from 2 L for surface samples to 11 L within the water column. After filtration, filter holders were disconnected from the GO-FLO bottles and a gentle vacuum was applied using a syringe in order to remove any

residual water under a laminar flow hood. Filters were then removed from the filter holders with plastic tweezers (which were rinsed with Milli-Q between samples). Most of the remaining seawater was removed via 'sipping' by capillary action, when placing the non-sampled side of the filter onto a clean 47 mm supor filter. Each filter pair was then placed in an acid-cleaned polystyrene PetriSlide (Millipore), double bagged, and finally stored at -20 °C until analysis at LEMAR. Between casts, filter holders were thoroughly rinsed with Milli-Q, placed in an acid bath (5% Trace metal grade HCl) for 24 hours, then rinsed with Milli-Q.

At each station, process blanks were collected as follows: 2 L of a deep (1000 m) and a shallow (40 m) seawater sample were first filtered through a 0.2 µm pore size capsule filter (Pall Gelman Acropak 200) mounted on to the outlet of the GO-FLO bottle before passing through the particle sampling filter, which was attached directly to the swinnex filter holder.

2.3. Analytical methods

In the home laboratory, sample handling was performed inside a clean room (Class 100). All solutions were prepared using ultrapure water (Milli-Q) and all plasticware had been acid-cleaned before use. Frozen filters, collected within the mixed layer or within nepheloid layers, were first cut in half using a ceramic blade: one filter half was dedicated to total digestion (see below), while the other half was archived at -20 °C for SEM analyses or acid leaching of "labile" metals following Berger et al. (2008) method (to be published separately).

Filters were digested following the method described in Planquette and Sherrell (2012). Filters were placed on the inner wall of acid-clean 15 mL PFA vials (Savillex^{TM}), and 2 mL of a solution containing 2.9 mol L^{-1} hydrofluoric acid (HF, suprapur grade, Merck) and 8 mol L^{-1} nitric acid (HNO_3, Ultrapur grade, Merck) was added to each vial. Vials were then closed and refluxed at 130 °C on a hot plate for 4 hours, after which the filters were removed. After cooling, the digest solution was evaporated at 110 °C to near dryness. Then, 400 µL of concentrated HNO_3 (Ultrapur grade, Merck) was added, and the solution was re-evaporated at 110 °C. Finally, the obtained residue was dissolved with 3 mL of 0.8 mol L^{-1} HNO_3 (Ultrapure grade, Merck). This archived solution was transferred to an acid cleaned 15 mL polypropylene centrifuge tube (Corning®) and stored at 4 °C until analyses.

All analyses were performed on a sector field inductively coupled plasma mass spectrometer (SF-ICP-MS Element 2, Thermo-Fisher Scientific). Samples were diluted by a factor of 7 on the day of analysis in acid-washed 13 mm (outer diameter) rounded bottom, polypropylene centrifuge tubes (VWR) with 0.8 mol L^{-1} HNO_3 (Ultrapur grade, Merck) spiked with 1µg L^{-1} of indium (^{115}In) solution in order to monitor the instrument drift. Samples were introduced with a PFA-ST nebulizer connected to a quartz cyclonic spray chamber (Elemental Scientific Incorporated, Omaha, NE) via a modified SC-Fast introduction system consisting of an SC-2 autosampler, a six-port valve and a vacuum-rinsing pump. The autosampler was contained under a HEPA filtered unit (Elemental Scientific). Two 6-point, matrix-matched multi-element standard curves with concentrations bracketing the range of the samples were run at the beginning, the middle and the end of each analytical run. Analytical replicates were made every 10 samples, while accuracy was determined by performing digestions of the certified reference material BCR-414 (plankton, Community Bureau of Reference, Commission of the European Communities), PACS-3 and MESS-4 (marine sediments, National Research Council Canada), following the same protocol used for the samples. Recoveries were typically within 10% of the certified values (and within the error of the data, taken from replicate measurements, Table 1). Once all data were normalized to an ^{115}In internal standard and

quantified using an external standard curve, the dilution factor of the total digestion was accounted for. The elemental concentrations were obtained per filter (pmol/filter) and were then process blank-corrected. Finally, pmol/filter values were divided by the volume of water filtered through stacked filters.

Total concentrations (sum of small size fraction (0.45-5 µm) and large (>5 µm) size fraction) of particulate trace elements are reported in Table S1.

2.4. Positive matrix factorisation

Positive Matrix Factorisation (PMF) was run to characterise the main factors influencing the particulate trace element variance along the GEOVIDE section. In addition to PFe, PAl, PMn, and PP, nine additional elements were included in the PMF: yttrium (Y), barium (Ba), lead (Pb), thorium (Th), titanium (Ti), vanadium (V), cobalt (Co), copper (Cu) and zinc (Zn). The PMF was conducted on samples where all elements were above their detection limits; after selection, 445 of the 549 existing data points were used. Analyses were performed using the PMF software, EPA PMF 5.0, developed by the USA Environmental Protection Agency (EPA). Three to six factor models were run on the data. The configuration that provided the lowest error estimation (i.e. was the most reliable) was the four factor model. To ensure stability, this model was run 100 times. After displacement, error estimation and bootstrap error estimation, the model was recognised as stable.

2.5. Derived and ancillary parameters

To investigate the proportion of lithogenic iron within the bulk particulate iron, we used the Upper Continental Crust (UCC) Fe/Al molar ratio (0.21) of Taylor and McLennan (1995) to calculate the lithogenic components of particles ($\%PFe_{litho}$) following Eq. (1):

$$\%\mathrm{PFelitho} = 100 * \left(\frac{\mathrm{PAl}}{\mathrm{PFe}}\right)\mathrm{sample} * \left(\frac{\mathrm{PFe}}{\mathrm{PAl}}\right)\mathrm{UCCratio} \quad (1)$$

The non-lithogenic PFe is obtained using Eq. (2):

$$\%\mathrm{PFenon\_litho} = 100 - \%\mathrm{PFelitho} \quad (2)$$

Note that while the $\%PFe_{litho}$ and $\%PFe_{non\text{-}litho}$ proxies are interesting tools to evaluate the importance of lithogenic and non-lithogenic (either biogenic or authigenic) fraction, they have to be used carefully, as the spatial and temporal variation of the lithogenic component ratios may involve uncertainties of the estimated fraction value.

In addition to PAl, PMn can be used as a tracer of inputs from shelf resuspension (Lam and Bishop, 2008), using a percentage of sedimentary inputs "%bulk sediment inputs" estimated according to the following equation:

$$\%\mathrm{bulksedimentPMn} = 100 * \left(\frac{\mathrm{PAl}}{\mathrm{PMn}}\right)\mathrm{sample} * \left(\frac{\mathrm{PMn}}{\mathrm{PAl}}\right)\mathrm{UCCratio} \quad (3)$$

with PAl/PMn being the ratio from the GEOVIDE samples and the PMn/PAl being the UCC value (0.0034; Taylor and McLennan, 1995).

This proxy can be a good indicator of sediment resuspension. We assume that particles newly resuspended in the water column will have the same PMn/PAl ratio as the UCC ratio, leading to a "%bulk sediment Mn" of 100%. This proxy assumes homogeneity of the sediment PMn/PAl ratio throughout the GEOVIDE section. However, this may not be the case at every station. In consequence, this proxy should only be used to identify new benthic resuspension at specific locations; inter-comparison between several locations may not be appropriate. When a sample presents a "%bulk sediment Mn" greater than 100%, we have assigned a maximum value of 100%. As the Mn cycle can also be influenced by biotic uptake (e.g. Peers and Price, 2004; Sunda and Huntsman, 1983), this proxy is only used at depths where biologic activity was negligible (i.e. below 150m depth).

Potential temperature ($\theta°$), salinity (S), and transmissometry data were retrieved from the CTD sensors (CTD SBE911 equipped with a SBE43).

3. Results

3.1. Hydrography setting

Here, we briefly describe the hydrography encountered during the GEOVIDE section (Figure 2) as a thorough description is available in García-Ibáñez et al. (2015). At the start of the section, the warm and salty Mediterranean Water (MW, S = 36.50, $\theta°$ = 11.7 °C) was sampled between 600 and 1700 m in the Iberian Abyssal Plain (IAP). MW resulted from the mixing between the Mediterranean Overflow Water (MOW) plume coming from the Mediterranean Sea and local waters. Surface water above the Iberian Shelf was characterised by low salinity (S = 34.95) at station 2 and 4 compared to surrounding water masses. Close to the sea floor of the Iberian Abyssal Basin, the North East Atlantic Deep Water (NEADW, S = 34.89, $\theta°$ = 2.0 °C) spread northward. The North Atlantic Central Water (NACW, S > 35.60, $\theta°$ > 12.3 °C) was the warmest water mass of the transect and was observed in the subsurface layer of the Western European Basin and Iberian Abyssal Plain. An old Labrador Sea Water (LSW, S = 34.87, $\theta°$ = 3.0 °C) flowed inside the Western European and Icelandic Basins, between 1000 and 2500m depth.

In the Icelandic Basin, below the old LSW, the Iceland-Scotland Overflow Water (ISOW, S = 34.98, $\theta°$ = 2.6 °C) spread along the Reykjanes Ridge slope. This cold water, originating from the Arctic, led to the formation of NEADW after mixing with surrounding waters. North Atlantic hydrography was impacted by the northward flowing of the North Atlantic Current (NAC), which carried warm and salty waters from the subtropical area. Due to air-sea interactions and mixing with surrounding water, the NACW is cooled and freshened in the subpolar gyre and is transformed in Subpolar Mode Water (SPMW). The formation of SPMW inside the Icelandic and Irminger Basins leads to the formation of regional mode waters: the Iceland Subpolar Mode Water (IcSPMW, S = 35.2, $\theta°$ = 8.0 °C) and the Irminger Subpolar Mode Water (IrSPMW, S = 35.01, $\theta°$ = 5.0 °C), respectively. IcSPMW was a relatively warm water mass with potential temperature up to 7 °C (García-Ibáñez et al., 2015). Another branch of the NAC mixed with Labrador Current waters to form the relatively fresh SubArctic Intermediate Water (SAIW, S =< 34.8, 4.5 °C < $\theta°$ < 6 °C).

The Irminger Basin is a complex area with a multitude of water masses. In the middle of the basin, an old LSW, formed one year before (Straneo et al., 2003), spread between 500 and 1200 m depth. Close to the bottom, the

Denmark Strait Overflow Water (DSOW, S = 34.91) flowed across the basin. Greenland coastal waters were characterised by low salinity values, down to S = 33. The strong East Greenland Current (EGC) flowed southward along the Greenland shelf in the Irminger Basin. At the southern tip of Greenland, this current enters the Labrador Basin along the west coast of Greenland and followed the outline of the basin until the Newfoundland shelf. In the Labrador Basin, the deep convection of SPMW at 2000 m was involved in the formation of the LSW (S = 34.9, $\theta°$ = 3.0°C) (García-Ibáñez et al., 2015; Yashayaev and Loder, 2009). Above the Newfoundland Shelf, surface waters were affected by discharge from rivers and ice-melting and characterised by extremely low salinity for open ocean waters, below 32 in the first 15 meters.

3.2. Section overview

Total particulate concentrations spanned a large range of concentrations from below detection (Table 1) to 304 nmol L^{-1} for PFe, 1544 nmol L^{-1} for PAl, 3.5 nmol L^{-1} for PMn and 402 nmol L^{-1} for PP. The ranges of concentrations are comparable to other studies recently published (Table 2).

Along the section, PFe, PAl, and PMn were predominantly found (> 90 %) in particles larger than 5 µm, except in surface waters, reflecting a more heterogenous pattern, where 9 ± 8.6 % of PFe, 10.9 ± 15.4 % of PAl and 32.8 ± 16.6 % of PMn , 38.8 ± 8.6 % of PP were hosted by smaller particles (0.45-5 µm). Data are shown in Figure 3.

3.3. Open Ocean stations: from the Iberian Abyssal Plain to the Labrador Basin

This concerns all stations from station 11 to 77, with the exception of stations 53, 56 and 61 which were sampled close to the Greenland coast (Figure 1). Particulate iron concentration profiles showed identical patterns at all the open ocean stations encountered along the section. Median PFe was low at 0.25 nmol L^{-1} within the first 100 m and steadily increased with depth. However, at two stations, elevated concentrations were determined in the upper 100 m, up to 4.4 nmol L^{-1} at station 77 at 40 m depth and 7 nmol L^{-1} at station 63 between 70 and 100 m depth. PFe concentrations gradually increased with depth, with a median PFe of 1.74 nmol L^{-1} below 1000m. Close to the seafloor of some stations (26, 29, 32, 34, 49, 60, and 71), high concentrations of PFe were observed, up to 88 nmol L^{-1} (station 71 at 3736 m). These high PFe values were associated with low beam transmissometry values ≤ 97 %.

Particulate aluminium and manganese profiles were similar to PFe profiles, with low concentrations measured in the first 100 m (1.88 nmol L^{-1} and 55 pmol L^{-1}, respectively) which increased towards the seafloor. Close to the seafloor, high concentrations were determined at the same stations cited above for PFe, with a maximum of 264 nmol L^{-1} and 3.5 nmol L^{-1} for PAl and PMn respectively at station 71 (supplementary Table S1). Highest particulate phosphorus concentrations were in the uppermost 50 m, with a median value of 66 nmol L^{-1}. Below 200 m depth PP concentrations decreased to values below 10 nmol L^{-1}. Inter-basins differences were observed within surface samples, with median PP concentration being higher in the Irminger Basin (127 nmol L^{-1}) than in the Iberian Abyssal Plain (28 nmol L^{-1}) (Figure 3).

Finally, above the Reykjanes Ridge, PP, PMn, PAl and PFe concentrations were in the same range as the surrounding open ocean stations. However, close to the seafloor, high concentrations were measured, with PFe,

PAl, and PMn reaching 16.2 nmol L^{-1}, 28.8 nmol L^{-1}, and 0.51 nmol L^{-1} at 1354 m depth, respectively (Figure 3 and Table S1).

3.4. Margins and Shelves: Iberian Margin (stations 1 to 4), Greenland coast (stations 53, 56 and 61) and Newfoundland Shelf (station78)

The Iberian margin was characterised by low beam transmissometry values at station 2 (88 % at 140 m depth, Figure 4a) suggesting high particle concentrations. Particulate iron concentrations varied from 0.02 nmol L^{-1} to 304 nmol L^{-1}. Within the first 50 m, PFe concentrations decreased towards the shelf break where PFe dropped from 2.53 nmol L^{-1} (station 2) to 0.8 nmol L^{-1} (Station 1). At all three stations, PFe concentrations increased with depth and reached a maximum close to the seafloor. For example, 300 nmol L^{-1} of PFe was determined at 138.5 m depth at station 2. Lithogenic tracers, such as PAl or PMn, presented similar profiles to PFe with concentrations ranging from 0.11 and 1544 nmol L^{-1}, and from below detection limit to 2.51 nmol L^{-1}, respectively (Figure 3, Table S1). Total particulate phosphorus concentrations were relatively low in surface waters ranging from values below detection to 38 nmol L^{-1}; concentrations decreased with depth and were less than 0.7 nmol L^{-1} below 1000 m depth.

In the vicinity of the Greenland shelf, PFe concentrations had a high median value of 10.8 nmol L^{-1} and were associated with high median PAl and PMn concentrations of 32.3 nmol L^{-1} and 0.44 nmol L^{-1}, respectively. Concentrations of PP were high at the surface with a value of 197 nmol L^{-1} at 25 m depth of station 61. Then, PP concentrations decreased strongly, to less than 30 nmol L^{-1} below 100 meters depth. Furthermore, beam transmissometry values in surface waters at these three stations, were the lowest of the entire section, with values below 85 % (Figure 4a).

Close to the Newfoundland margin, surface waters displayed a small load of particulate trace metals as PFe, PAl, and PMn concentrations were below 0.8 nmol L^{-1}, 2 nmol L^{-1}, and 0.15 nmol L^{-1}, respectively. Then, close to the bottom of station 78, at 371 m depth, beam transmissometry values dropped to 94 % (Figure 4a) and were associated with extremely high concentrations of PFe = 168 nmol L^{-1}, PAl = 559 nmol L^{-1}, and PMn = 2 nmol L^{-1}. Total PP concentrations in the first 50 m ranged from 35 to 97 nmol L^{-1}. Below 50 m, PP remained relatively high with values up to 16 nmol L^{-1} throughout the water column. (Figure 3 and Table S1).

4. Discussion

Our goal was to investigate mechanisms that drive the distribution of PFe in the North Atlantic, in particular the different routes of supply and removal. Possible sources of PFe include lateral advection offshore from margins, atmospheric inputs, continental run-off, melting glaciers and icebergs, resuspended sediments, hydrothermal inputs and biological uptake. Removal processes include remineralization, dissolution processes and sediment burial.

In the following sections, we examine each of these sources and processes, explore the evidence for their relative importance, and use compositional data to estimate the particle types and host phases for iron and associated elements.

4.1. Analysis of the principal factors controlling variance: near-ubiquitous influence of crustal particles in the water column

Positive matrix factorisation analysis (Figure 5) was undertaken on the entire dataset, in consequence, the factors described below are highly influenced by the major variations of particulate element concentrations (usually at the interfaces, i.e. margin, seafloor, surface layer). The first factor is characterised by lithogenic elements, representing 86.8 % of the variance of PFe, 75.8 % of PAl and 90.5 % of PTi. The second factor is correlated with both Mn and Pb and explains no less than 76.5 % and 77.0 % of their respective variances. Ohnemus and Lam (2015) observed this co-relation between manganese and lead particles and explained it by the co-transport on Mn-oxides (Boyle et al., 2005). The formation of barite explains the third factor and constrained 87.7 % of the Ba variance in the studied regions. Biogenic barite accumulation within the mesopelagic layer is related to bacterial activity and remineralisation of biogenic material (Lemaitre et al., 2018a). A biogenic component is the fourth factor and explained most of PP variance, 83.7 %. The micronutrient trace metals, copper, cobalt and zinc, had more than a quarter of their variances influenced by this factor. Note that the biogenic contribution to PFe and other trace elements will be discussed in another paper (Planquette et al., in prep).

These results indicate that along the GA01 section, PFe distributions were predominantly controlled by lithogenic material and to a smaller extent by remineralisation processes (PMF, factor 3 = 4.1 %). This does not rule out some biogenic influences on PFe distribution, especially in the surface, but its contribution is most likely obscured by the high lithogenic contribution.

To further investigate the influence of crustal material on the distribution of PFe, it is instructive to examine the distribution of the PFe to PAl molar ratio, and the resulting $\%PFe_{litho}$ (see section 2.6 for definition of this parameter) along the section (Figure 6). Overall, the estimated lithogenic contribution to PFe varies from 25 % (west of the Irminger Basin, station 60, 950 m depth) to 100 % at stations located within the Western European Basin. Note that 100% of estimated lithogenic PFe does not necessary mean that biogenic particles are absent; they may just be masked by the dominance of lithogenic particles. Important inter-basin variations are observed along the section (Figure 6). The IAP and WEB displayed high median values of the proxy $\%PFe_{litho}$, 90 % (Figure 6b); this could be linked to the lateral advection of iron rich lithogenic particles sourced from the Iberian margin and to atmospheric inputs (Shelley et al., 2017). Then, between stations 26 and 29, the $\%PFe_{litho}$ proxy values dramatically decreased, and reached values less than 55 % in the Iceland, Irminger and the Labrador basins (Figure 6b). This feature is likely associated with the presence of the Sub-Arctic Front located between 49.5 and 51 °N latitude and 23.5 and 22 °W longitude (Zunino et al., 2017). Indeed, this front which separates cold and fresh water of subpolar origin from warm and salty water of subtropical origin was clearly identifiable by the steep gradient of the isohalines between station 26 and 29; salinity dropping from 35.34 to 35.01 (Figure 2). Lower $\%PFe_{litho}$ proxy values, could be associated with higher proportions of PFe from biogenic origin, especially in the case of the LSW.

4.2. Tracking the different inputs of particulate iron

4.2.1. Inputs at margins: Iberian, Greenland and Newfoundland

Inputs of iron from continental margin sediments supporting the high productivity found in shallow coastal regions have been demonstrated in the past (e.g. Cullen et al. 2009, Elrod et al. 2004, Jeandel et al. 2011, Ussher et al. 2007) and sometimes, were shown to be advected at great distances from the coast (e.g. Lam and Bishop, 2008). In the following section, we will investigate these possible sources in proximity to the different margins encountered.

The Iberian margin

The Iberian margin was an important source of lithogenic-derived iron-rich particles to the Atlantic Ocean during GEOVIDE; shelf resuspension impacts were perceptible up to 280 km from the margin (Station 11) in the Iberian Abyssal Plain (Figure 8).

On the shelf, at station 2, high sediment resuspension resulted in the low beam transmissometry value (87.6 %) at the immediate vicinity of the seafloor (153 m depth). This sediment resuspension led to an extensive input of lithogenic particles within the water column associated with high concentrations of PFe (304 nmol L^{-1}), PAl (1500 nmol L^{-1}), and PMn (2.5 nmol L^{-1}) (Figure 3, Table S1). Moreover, 100 % of PFe was estimated to have a lithogenic origin (Figure 8b) while 100 % of the PMn was estimated to be the result of a recent sediment resuspension according to the $\%PFe_{litho}$ and "%bulk sediment Mn" proxies (Figure 8b and c), confirming the resuspended particle input. In addition, ADCP data acquired during GEOVIDE (Zunino et al., 2017) and several other studies have reported an intense current spreading northward coming from the Straits of Gibraltar and Mediterranean Sea, leading to the strong resuspension of benthic sediments above the Iberian Shelf (e.g. Biscaye and Eittreim, 1977, Eittreim et al., 1976, McCave and Hall, 2002, Spinrad et al., 1983).

At distance from the shelf, within the Iberian Abyssal Plain, an important lateral advection of PFe from the margin was observable (Figure 8a). These lateral inputs occurred at two depth ranges: between 400 and 1000 m as seen at stations 4 and 1, with PFe concentrations reaching 4 nmol L^{-1}, and between 2500 m and the bottom (3575 m) of station 1, with PFe concentrations reaching 3.5 nmol L^{-1}. While 100 % of PFe had a lithogenic signature, the sedimentary source input estimation decreased, between 40 % and 90 % of the PMn (Figure 8b). Transport of lithogenic particles was observable until station 11 (12.2°W) at 2500 m where PFe concentration was 7.74 nmol L^{-1} and 60 % of PMn had a sedimentary origin (Figure 4). It is noteworthy that no increase in PFe, PMn or PAl was observed between 500 and 2000 m depth, where the MOW spreads (García-Ibáñez et al., 2015). This is consistent with the observed dissolved iron (DFe) concentrations (Tonnard et al., 2018, this issue), yet in contrast to dissolved aluminium (DAl) concentrations (Menzel-Barraqueta et al., 2018, this issue) which were high in the MOW, and with the study of Ohnemus and Lam (2015) that reported a maximum PFe concentration at 695 m depth associated with the particle-rich Mediterranean Overflow Water (Eittreim et al., 1976) in the IAP. However, their station was located further south of our station 1. The shallower inputs observed at stations 1 and 4 could therefore be attributed to sediment resuspension from the Iberian margin and nepheloid layer at depth for station 1.

Surface coastal waters of the Iberian Shelf are impacted by the runoff for the Tagus River, which is characterised by high suspended matter discharges, ranging between 0.4 to 1×10^6 tons yr^{-1}, and with a high anthropogenic trace element signature (Jouanneau et al., 1998). During the GEOVIDE section, the freshwater input was observable at stations 1, 2 and 4 in the first 20 m; salinity was below 35.2 while surrounding water masses had

salinity up to 35.7. Within the freshwater plume, particulate concentrations were high at station 2 with PFe of 1.83 nmol L^{-1}. Further away from the coast, the particulate concentrations remained low at 20m depth, with PFe, PAl, and PMn concentrations of 0.77 nmol L^{-1}, 3.5 nmol L^{-1}, and 0.04 nmol L^{-1}, respectively at station 1. The low expansion of the Tagus plume is likely due to the rapid settling of suspended matter. Indeed, our coastal station 2 was located approximately 50 km from the Iberian coast, whereas the surface particle load can only be observed at a maximum distance of 30 km from the Tagus estuary (Jouanneau et al., 1998), Overall, the Iberian margin appears to be an important source of lithogenic-derived iron rich particles to the Atlantic Ocean.

South Greenland

During GEOVIDE, the Greenland shelves were a source of particulate-rich meteoric water leading to a transfer of DFe to PFe by enhanced biological activity. Indeed, both East (station 53) and West (station 61) Greenland shelves had high concentration of particles (beam transmissometry of 83 %, Figure 4a) and particulate trace elements, reaching 22.1 nmol L^{-1} (at 100 m depth) and 18.7 nmol L^{-1} (at 136 m depth) of PFe, respectively. Several studies have already demonstrated the importance of icebergs and sea ice melting as sources of dissolved and particulate iron (e.g. van der Merwe et al., 2011a, 2011b; Planquette et al., 2011; Raiswell et al., 2008). The Greenland shelf is highly influenced by external fresh water inputs such as sea-ice-melting or riverine runoff (Fragoso et al., 2016), which are important sources of iron to the Greenland Shelf (Bhatia et al., 2013; Hawkings et al., 2014; Statham et al., 2008). During the cruise, the relative freshwater observed ($S < 33$ psu) within the first 25 m of stations 53 and 61 was associated with high PFe (19 nmol L^{-1}), PAl (61 nmol L^{-1}), PMn (0.6 nmol L^{-1}) and low beam transmissometry ($\leq 85\%$) (Figure 4a and Table S1). The associated particles were enriched in iron compared to aluminium, as PFe/PAl ratio was 0.3 within the meteoric water plume. The high PP concentrations (reaching 197 nmol L^{-1}) resulting from high biological production (Chl-a = 6.21 mg m^{-3} at 24 m at station 61), induced by the supply of bioavailable dissolved iron (surface DFe of 0.79 nM at station 61) from meteoric water (Raiswell et al., 2008; Statham et al., 2008; Tonnard et al. 2018), led to a transfer of DFe to the particulate phase. This is in line with the finding that around 30 % PFe had a non-lithogenic origin. In addition, only 40% PMn originated from resuspended sediments. Interestingly, these two proxies remained constant from the seafloor to the surface (Station 49, Figure 8), with around 25 % of the PMn of sedimentary origin, which could be due to important mixing occurring on the shelf. The lithogenic PFe could result from the release of PFe from Greenland bedrock captured during the ice sheet formation on land.

The spatial extent of the off-shelf lateral transport of particles was not important on the east Greenland coast. Indeed, no visible increase of particulate trace metal concentrations was visible at the first station off-shelf, station 60 (Figure 8), except at 1000 m depth, where a strong increase (up to 90 %) of sedimentary PMn was seen. This is probably due to the East Greenland Coastal Current (EGCC) that was located at station 53 which constrained these inputs while stations 56 and 60 were under the influence of another strong current, the East Greenland-Irminger current (EGIC) (Zunino et al., 2017). To the west of the Greenland margin, lateral transport of particles was slightly more important. Noticeable concentrations of particulate lithogenic elements were observable until station 64 located 125 km away from shoreline. These particles had a decreased PFe lithogenic contribution (50 %) with a similar (25 %) sedimentary PMn content than closer to the margin (Figure 8b and c). The increasing nature of non-lithogenic PFe is linked to the bloom in surface waters (PFe/PAl ratio of 0.30 mol mol^{-1}, PP of 197 nmol L^{-1} and Chl-a concentration of 6.21 mg m^{-3} at station 61), with the gravitational settling of biogenic PFe.

Therefore, particles newly resuspended from Greenland sediments are an important source, representing around one third of the pMn pool, combined with surface inputs such as riverine runoff and/or ice-melting that are delivering particles on the shelf, and also biological production. Unlike the Iberian shelf, the Greenland margin was not an important provider of particulate metals inside the Irminger and Labrador Basins, due to the circulation that constrained the extent of the margin plume.

The Newfoundland Shelf

Previous studies have already described the influence of fresh water on the Newfoundland shelf from the Hudson Strait and/or Canadian Artic Archipelago (Fragoso et al., 2016; Yashayaev, 2007). Yashayaev (2007) also monitored strong resuspension of sediments associated with the spreading of the Labrador Current along the West Labrador margin.

Close to the Newfoundland coastline, at station 78, high fresh water discharge (≤ 32 psu) was observed in surface waters (Benetti et al., 2017). Interestingly, these freshwater signatures were not associated with elevated particulate trace metal concentrations. Distance of meteoric water sources implied a long travel time for the water to spread through the Labrador Basin to our sampling stations. Along the journey, particles present originally may have been removed from the water column by gravitational settling.

The proportion of lithogenic PFe was relatively high and constant throughout the water column, with a median value of 70 %. At station 78, 95 % of the PMn had a sedimentary origin close to the seafloor (371 m). The spreading of the recent sediment resuspension was observable until 140 m depth where the contribution of sedimentary Mn was still 51% (Figure 8c, Table S2). This could correspond to an intense nepheloid layer as previously reported by Biscaye and Eittreim (1977) (see also section 3.3.2). The high PFe concentration (184 nmol L^{-1}, station 78, 371 m depth, Figure 8b) associated with a high percentage of sedimentary PMn (95%) observed at the bottom of this station, was therefore the result of an important resuspension of shelf sediments. This was confirmed with low transmissometry values of 95 % (Figure 4a).

Along the GEOVIDE section, continental shelves provided an important load of particles to the surrounding water column. The three margins sampled during GEOVIDE behaved very differently; the Iberian margin discharged high quantities of lithogenic particles far from the coast while the Greenland and Newfoundland margins did not reveal important PFe concentrations. Spreading of particles is tightly linked to hydrodynamic conditions, which in the case of the Greenland margin, prevented long distance seeding of PFe. Moreover, each margin showed a specific PFe/PAl ratio (Figure 9) indicating different composition of the resuspended particles. Resuspended particles represent the composition of sediment at the margin if redox transformation of iron and aluminium are considered negligible under these circumstances. Differences between margins were due to the presence of non-crustal particles, either biogenic or authigenic. Biological production in surface waters and authigenic formation of iron hydroxide produced particles with a higher PFe/PAl content and their export through the water column to the sediment increased the PFe/PAl ratio at depth. Regions where biological production is intense such as in the vicinity of Newfoundland presented higher PFe/PAl ratios of resuspended benthic particles.

4.2.2 Benthic resuspended sediments

Along the GEOVIDE section, Benthic nepheloid layers (BNLs) provided high concentrations of particulate trace elements to the deep open ocean, contributing significantly to the total budget of iron. BNLs were observable in each province, although intensities varied (Figures 3 and 10).

In BNLs located within the WEB, PFe concentrations reached up to 10 nmol L^{-1} (stations 26 and 29, Figure 10a; Table S1). These concentrations were lower than PFe concentrations in BNLs from the Icelandic (stations 32 and 34), Irminger (stations 42 and 44) and Labrador Basins (stations 68, 69 and 71), where benthic resuspension led to PFe concentrations higher than 40 nmol L^{-1}, even reaching 89 nmol L^{-1} at the bottom of station 71 (3736 m depth). Moreover, in the Irminger and Labrador Basins, PFe/PAl molar ratios within BNLs were higher than the ones measured within the WEB at station 26 and 29. In the Irminger Basin, PFe/PAl reached 0.4 mol mol^{-1} (Figure 10b), which could reveal a mixture of lithogenic and biogenic matter that had been previously exported. This feature was also observed in the Labrador Basin, with PFe/PAl ratio ranging between 0.34 and 0.44 mol mol^{-1}. In contrast, BNLs sampled in the WEB clearly have a lithogenic imprint, with PFe/PAl molar ratios close to the crustal one. Resuspended sediments with a non-crustal contribution seem to have higher PFe contents than sediments with lithogenic characteristics. Nevertheless, interestingly all BNLs present during GEOVIDE were spreading identically, with impacts observable up to 200 m above the oceanic seafloor (Figure 10), as reflected in beam transmissometry values, and PFe concentrations, which returned to background levels at 200 m above the seafloor. The presence of these BNLs has also been reported by Le Roy et al. (2018) using radium-226 activity. Important differences of PFe intensities could also be due to different hydrographic components and topographic characteristics. BNLs occur due to strong hydrographic stresses (i.e. boundary currents, benthic storms and deep eddies) interacting with the ocean floor (Biscaye and Eittreim, 1977; Eittreim et al., 1976; Gardner et al., 2017, 2018). They are, by definition, highly variable geographically and temporally, but we have no physical data which would allow us to investigate this hypothesis further.

4.2.3. Reykjanes Ridge inputs

Above the Reykjanes Ridge (Station 38), high PFe concentrations were determined, reaching 16 nmol L^{-1} just above the seafloor, while increased DFe concentrations were reported to the east of the ridge (Tonnard et al., 2018, this issue). The exact sources of iron-rich particles cannot be well constrained, as they could come from active hydrothermal vents or resuspension of particulate matter from new crustal matter produced at the ridge. According to the oceanic circulation (Zunino et al., 2017; Garcia-Ibanez et al., 2017), hydrothermal particles could have been seen in the ISOW within the Icelandic Basin. Nevertheless, at the vicinity of the ridge, scanning electron microscope (SEM) analyses of our samples did reveal several biological debris and clays but not the presence of iron (oxy-)hydroxide particles (supplementary figure S1), which are known to be produced close to hydrothermal vents (Elderfield and Schultz, 1996). Their absence could thus indicate an absence of vents. However, data from other proxies, such as helium-3, would be necessary to confirm the presence or absence of an hydrothermal source close to station 38.

4.2.4. Atmospheric inputs

Atmospheric deposition is an important source of trace elements in surface of the open ocean (e.g. Jickells et al., 2005). Atmospheric inputs, both wet and dry, were reported to be low during the GEOVIDE cruise (Menzel

Barraqueta et al., 2018b, this issue; Shelley et al., 2017; 2018). In fact, oceanic particle measurements in surface waters along the section did not reveal high PFe or PAl concentrations. One pattern is interesting to note: the surface waters of the Iberian Abyssal Plain and Western European Basin, between stations 11 and 23 presented a characteristic feature with really low PFe/PAl elemental ratios, of 0.11, smaller than the UCC ratio of 0.21 (Figure 6a). Such low ratios have been reported in the same region by Barrett et al. (2012). One possible explanation is given by Buck et al. (2010) who described Fe-depleted aerosols in this area of the North Atlantic with PFe/PAl ratio below UCC ratio. However, Shelley et al. (2017) found a higher PFe/PAl ratio around 0.25 is this area (their samples geoa5-6). This result, highlights some of the difficulties in linking atmospheric inputs to water column data (Baker et al., 2016), and implies a probable fractionation after aerosol deposition. In addition, there is high spatial and temporal variability of atmospheric deposition (Mahowald et al., 2005) and a certain degree of uncertainty about the dissolution processes of atmospherically-transported particles (Bonnet and Guieu, 2004).

5. Conclusions

The investigation of the PFe composition of suspended particulate matter along the GEOVIDE section in the North Atlantic reflects the pervasive influence of crustal particles, augmented by sedimentary inputs at margins, and within benthic nepheloid layers at depths. In consequence, variance of particulate iron along the section is mainly explained by lithogenic factors.

Resuspension of sedimentary particles from continental shelves are responsible of high particulate iron concentrations within the surrounding water column and could be observed at long distances from the shelf, in the case of the Iberian margin. Our results also demonstrate the impact of Arctic meteoric water on the Greenland shelf, while in surface waters, the enhancement of productivity by new bioavailable iron is leading to a transfer of dissolved iron to the particulate phase. Benthic nepheloid layer are providing important concentration of particles to the water column; they were observed in most of the oceanic basin encountered along the GEOVIDE section.

Overall, PFe distributions in the North Atlantic are strongly influenced by sources at its boundaries (i.e. continental margins and seafloor). When combined with other datasets from the GEOTRACES program in a modelling study, for example, use of this data will facilitate a greater understanding of particulate iron cycling in the North Atlantic.

Acknowledgments

We are greatly indebted to the captain and crew of the N/O Pourquoi Pas? for their help during the GEOVIDE mission and clean rosette deployment. We would like to give special thanks to Fabien Pérault and Emmanuel de Saint Léger for their technical expertise, to Catherine Schmechtig for the GEOVIDE database management and Greg Cutter for his guidance in setting up the new French clean sampling system. We would like to thank both reviewers for constructive comments that greatly improved this manuscript.

We also would like to thank Reiner Schlitzer for the Ocean Data View software (ODV).

This work was supported by the French National Research Agency (ANR-13-BS06-0014, ANR-12-PDOC-0025-01), the French National Centre for Scientific Research (CNRS-LEFE-CYBER), the LabexMER (ANR-10-LABX-19), and Ifremer. It was supported for the logistic by DT-INSU and GENAVIR.

References

Aguilar-Islas, A. M., Rember, R., Nishino, S., Kikuchi, T. and Itoh, M.: Partitioning and lateral transport of iron to the Canada Basin, Polar Sci., 7(2), 82–99, doi:10.1016/j.polar.2012.11.001, 2013.

Baker, A. R., Adams, C., Bell, T. G., Jickells, T. D. and Ganzeveld, L.: Estimation of atmospheric nutrient inputs to the Atlantic Ocean from 50°N to 50°S based on large-scale field sampling: Iron and other dust-associated elements, Global Biogeochem. Cycles, 27(3), 755–767, doi:10.1002/gbc.20062, 2013.

Baker, A. R., Landing, W. M., Bucciarelli, E., Cheize, M., Fietz, S., Hayes, C. T., Kadko, D., Morton, P. L., Rogan, N., Sarthou, G., Shelley, R. U., Shi, Z., Shiller, A. and van Hulten, M. M. P.: Trace element and isotope deposition across the air–sea interface: progress and research needs, Philos. Trans. R. Soc. A Math. Phys. Eng. Sci., 374(2081), 20160190, doi:10.1098/rsta.2016.0190, 2016.

Barrett, P. M., Resing, J. A., Buck, N. J., Buck, C. S., Landing, W. M. and Measures, C. I.: The trace element composition of suspended particulate matter in the upper 1000m of the eastern North Atlantic Ocean: A16N, Mar. Chem., 142–144, 41–53, doi:10.1016/j.marchem.2012.07.006, 2012.

Benetti, M., Reverdin, G., Lique, C., Yashayaev, I., Holliday, N. P., Tynan, E., Torres-Valdes, S., Lherminier, P., Tréguer, P., and Sarthou, G.: Composition of freshwater in the spring of 2014 on the southern Labrador shelf and slope, Journal of Geophysical Research: Oceans, 122, 1102-1121, 10.1002/2016jc012244, 2017.

Berger, C. J. M., Lippiatt, S. M., Lawrence, M. G. and Bruland, K. W.: Application of a chemical leach technique for estimating labile particulate aluminum, iron, and manganese in the Columbia River plume and coastal waters off Oregon and Washington, J. Geophys. Res., 113, C00B01, doi:10.1029/2007JC004703, 2008.

Bergquist, B. A., Wu, J. and Boyle, E. A.: Variability in oceanic dissolved iron is dominated by the colloidal fraction, Geochim. Cosmochim. Acta, 71(12), 2960–2974, doi:10.1016/j.gca.2007.03.013, 2007.

Bhatia, M. P., Kujawinski, E. B., Das, S. B., Breier, C. F., Henderson, P. B. and Charette, M. A.: Greenland meltwater as a significant and potentially bioavailable source of iron to the ocean, Nat. Geosci., 6(4), 274–278, doi:10.1038/ngeo1746, 2013.

Biscaye, P. E. and Eittreim, S. L.: Suspended Particulate Loads and Transports in the Nepheloid Layer of the Abyssal Atlantic Ocean, Dev. Sedimentol., 23(C), 155–172, doi:10.1016/S0070-4571(08)70556-9, 1977.

Bishop, J. K. B. and Biscaye, P. E.: Chemical characterization of individual particles from the nepheloid layer in the Atlantic Ocean, Earth Planet. Sci. Lett., 58(2), 265–275, doi:10.1016/0012-821X(82)90199-6, 1982.

Bishop, J. K. B. and Fleisher, M. Q.: Particulate manganese dynamics in Gulf Stream warm-core rings and surrounding waters of the N.W. Atlantic, Geochim. Cosmochim. Acta, 51(10), 2807–2825, doi:10.1016/0016-7037(87)90160-8, 1987.

Bonnet, S. and Guieu C.: Dissolution of atmospheric iron in seawater, Geophys. Res. Lett., 31(3), L03303, doi:10.1029/2003GL018423, 2004.

Boyle, E. A., Bergquist, B. A., Kayser, R. A. and Mahowald, N.: Iron, manganese, and lead at Hawaii Ocean Time-series station ALOHA: Temporal variability and an intermediate water hydrothermal plume, Geochim. Cosmochim. Acta, 69(4), 933–952, doi:10.1016/j.gca.2004.07.034, 2005.

Buck, C. S., Landing, W. M., Resing, J. A. and Measures, C. I.: The solubility and deposition of aerosol Fe and other trace elements in the North Atlantic Ocean: Observations from the A16N CLIVAR/CO2repeat hydrography section, Mar. Chem., 120(1–4), 57–70, doi:10.1016/j.marchem.2008.08.003, 2010.

Cheize, M., Planquette, H. F., Fitzsimmons, J. N., Pelleter, E., Sherrell, R. M., Lambert, C., Bucciarelli, E., Sarthou, G., Le Goff, M., Liorzou, C., Chéron, S., Viollier, E., and Gayet, N.: Contribution of resuspended sedimentary particles to dissolved iron and manganese in the ocean: An experimental study, Chemical Geology. doi: 10.1016/j.chemgeo.2018.10.003, 2018.

Collier, R. and Edmond, J.: The trace element geochemistry of marine biogenic particulate matter, Prog. Oceanogr., 13(2), 113–199, doi:10.1016/0079-6611(84)90008-9, 1984.

Cullen, J. T., Chong, M. and Ianson, D.: British columbian continental shelf as a source of dissolved iron to the subarctic northeast Pacific Ocean, Global Biogeochem. Cycles, 23(4), 1–12, doi:10.1029/2008GB003326, 2009.

Cutter, G. A. and Bruland, K. W.: Rapid and noncontaminating sampling system for trace elements in global ocean surveys, Limnol. Oceanogr. Methods, 10(JUNE), 425–436, doi:10.4319/lom.2012.10.425, 2012.

Dammshäuser, A., Wagener, T., Garbe-Schönberg, D. and Croot, P.: Particulate and dissolved aluminum and titanium in the upper water column of the Atlantic Ocean, Deep. Res. Part I Oceanogr. Res. Pap., 73, 127–139, doi:10.1016/j.dsr.2012.12.002, 2013.

Dehairs, F., Jacquet, S., Savoye, N., Van Mooy, B. A. S., Buesseler, K. O., Bishop, J. K. B., Lamborg, C. H., Elskens, M., Baeyens, W., Boyd, P. W., Casciotti, K. L. and Monnin, C.: Barium in twilight zone suspended matter as a potential proxy for particulate organic carbon remineralization: Results for the North Pacific, Deep. Res. Part II Top. Stud. Oceanogr., 55(14–15), 1673–1683, doi:10.1016/j.dsr2.2008.04.020, 2008.

Dutay, J. C., Tagliabue, A., Kriest, I. and van Hulten, M. M. P.: Modelling the role of marine particle on large scale 231Pa, 230Th, Iron and Aluminium distributions, Prog. Oceanogr., 133, 66–72, doi:10.1016/j.pocean.2015.01.010, 2015.

Eittreim, S., Thorndike, E. M. and Sullivan, L.: Turbidity distribution in the Atlantic Ocean, Deep. Res. Oceanogr. Abstr., 23(12), 1115–1127, doi:10.1016/0011-7471(76)90888-3, 1976.

Elderfield, H. and Schultz, A.: Mid-Ocean Ridge Hydrothermal Fluxes and the Chemical Composition of the Ocean, Annu. Rev. Earth Planet. Sci., 24(1), 191–224, doi:10.1146/annurev.earth.24.1.191, 1996.

Ellwood, M. J., Nodder, S. D., King, A. L., Hutchins, D. A., Wilhelm, S. W. and Boyd, P. W.: Pelagic iron cycling during the subtropical spring bloom, east of New Zealand, Mar. Chem., 160, 18–33, doi:10.1016/j.marchem.2014.01.004, 2014.

Elrod, V. A., Berelson, W. M., Coale, K. H. and Johnson, K. S.: The flux of iron from continental shelf sediments: A missing source for global budgets, Geophys. Res. Lett., 31(12), 2–5, doi:10.1029/2004GL020216, 2004.

Fitzwater, S. E., Johnson, K. S., Gordon, R. M., Coale, K. H. and Smith, W. O.: Trace metal concentrations in athe Ross Sea and their relationship with nutrients and phytoplankton growth, Deep. Res. Part II Top. Stud. Oceanogr., 47(15–16), 3159–3179, doi:10.1016/S0967-0645(00)00063-1, 2000.

Fragoso, G. M., Poulton, A. J., Yashayaev, I. M., Head, E. J. H., Stinchcombe, M. C. and Purdie, D. A.: Biogeographical patterns and environmental controls of phytoplankton communities from contrasting hydrographical zones of the Labrador Sea, Prog. Oceanogr., 141, 212–226, doi:10.1016/j.pocean.2015.12.007, 2016.

Frew, R. D., Hutchins, D. A., Nodder, S., Sanudo-Wilhelmy, S., Tovar-Sanchez, A., Leblanc, K., Hare, C. E. and Boyd, P. W.: Particulate iron dynamics during FeCycle in subantarctic waters southeast of New Zealand, Global Biogeochem. Cycles, 20(1), 1–15, doi:10.1029/2005GB002558, 2006.

García-Ibáñez, M. I., Pardo, P. C., Carracedo, L. I., Mercier, H., Lherminier, P., Ríos, A. F. and Pérez, F. F.: Structure, transports and transformations of the water masses in the Atlantic Subpolar Gyre, Prog. Oceanogr., 135, 18–36, doi:10.1016/j.pocean.2015.03.009, 2015.

Gardner, W. D., Tucholke, B. E., Richardson, M. J. and Biscaye, P. E.: Benthic storms, nepheloid layers, and linkage with upper ocean dynamics in the western North Atlantic, Mar. Geol., 385, 304–327, doi:10.1016/j.margeo.2016.12.012, 2017.

Gardner, W. D., Richardson, M. J. and Mishonov, A. V.: Global assessment of benthic nepheloid layers and linkage with upper ocean dynamics, Earth Planet. Sci. Lett., 482, 126–134, doi:10.1016/j.epsl.2017.11.008, 2018.

Gerringa, L. J. A., Rijkenberg, M. J. A., Schoemann, V., Laan, P. and de Baar, H. J. W.: Organic complexation of iron in the West Atlantic Ocean, Mar. Chem., 177, 434–446, doi:10.1016/j.marchem.2015.04.007, 2015.

Hawkings, J. R., Wadham, J. L., Tranter, M., Raiswell, R., Benning, L. G., Statham, P. J., Tedstone, A., Nienow, P., Lee, K. and Telling, J.: Ice sheets as a significant source of highly reactive nanoparticulate iron to the oceans, Nat. Commun., 5(May), 1–8, doi:10.1038/ncomms4929, 2014.

Hwang, J., Druffel, E. R. M. and Eglinton, T. I.: Widespread influence of resuspended sediments on oceanic particulate organic carbon: Insights from radiocarbon and aluminum contents in sinking particles, Global Biogeochem. Cycles, 24(4), 1–10, doi:10.1029/2010GB003802, 2010.

637 Jeandel, C. and Oelkers, E. H.: The influence of terrigenous particulate material dissolution on ocean chemistry
638 and global element cycles, Chem. Geol., 395, 50–66, doi:10.1016/j.chemgeo.2014.12.001, 2015.

639 Jeandel, C., Peucker-Ehrenbrink, B., Jones, M. T., Pearce, C. R., Oelkers, E. H., Godderis, Y., Lacan, F., Aumont,
640 O. and Arsouze, T.: Ocean margins: The missing term in oceanic element budgets?, Eos, Transactions American
641 Geophysical Union, 92(26), 217–224, doi: 10.1029/2011EO260001, 2011.

642 Jickells, T. D., An, Z. S., Andersen, K. K., Baker, A. R., Bergametti, C., Brooks, N., Cao, J. J., Boyd, P. W., Duce,
643 R. A., Hunter, K. A., Kawahata, H., Kubilay, N., LaRoche, J., Liss, P. S., Mahowald, N., Prospero, J. M.,
644 Ridgwell, A. J., Tegen, I. and Torres, R.: Global iron connections between desert dust, ocean biogeochemistry,
645 and climate, Science (80-.)., 308(5718), 67–71, doi:10.1126/science.1105959, 2005.

646 Jouanneau, J. M., Garcia, C., Oliveira, A., Rodrigues, A., Dias, J. A. and Weber, O.: Dispersal and deposition of
647 suspended sediment on the shelf off the Tagus and Sado estuaries, S.W. Portugal, Prog. Oceanogr., 42(1–4), 233–
648 257, doi:10.1016/S0079-6611(98)00036-6, 1998.

649 Labatut, M., Lacan, F., Pradoux, C., Chmeleff, J., Radic, A., Murray, J. W., Poitrasson, F., Johansen, A. M., Thil,
650 F., Lacan, F., Pradoux, C., Chmeleff, J., Radic, A., Murray, J. W., Poitrasson, F., Johansen, A. M. and Thil, F.:
651 Iron sources and dissolved-particulate interactions in the seawater of the Western Equatorial Pacific, iron isotope
652 perspectives., Global Biogeochem Cycles, 1044–1065, doi:10.1002/2014GB004928, 2014.

653 Lam, P. J. and Bishop, J. K. B.: The continental margin is a key source of iron to the HNLC North Pacific Ocean,
654 Geophys. Res. Lett., 35(7), 1–5, doi:10.1029/2008GL033294, 2008.

655 Lam, P. J., Ohnemus, D. C. and Marcus, M. A.: The speciation of marine particulate iron adjacent to active and
656 passive continental margins, Geochim. Cosmochim. Acta, 80, 108–124, doi:10.1016/j.gca.2011.11.044, 2012.

657 Lam, P. J., Ohnemus, D. C. and Auro, M. E.: Size-fractionated major particle composition and concentrations
658 from the US GEOTRACES North Atlantic Zonal Transect, Deep. Res. Part II Top. Stud. Oceanogr., 116, 303–
659 320, doi:10.1016/j.dsr2.2014.11.020, 2015.

660 Lam, P. J., Lee, J. M., Heller, M. I., Mehic, S., Xiang, Y. and Bates, N. R.: Size-fractionated distributions of
661 suspended particle concentration and major phase composition from the U.S. GEOTRACES Eastern Pacific Zonal
662 Transect (GP16), Mar. Chem., (April), 0–1, doi:10.1016/j.marchem.2017.08.013, 2017.

663 Lannuzel, D., Bowie, A. R., van der Merwe, P. C., Townsend, A. T. and Schoemann, V.: Distribution of dissolved
664 and particulate metals in Antarctic sea ice, Mar. Chem., 124(1–4), 134–146, doi:10.1016/j.marchem.2011.01.004,
665 2011.

666 Lannuzel, D., Van der Merwe, P. C., Townsend, A. T. and Bowie, A. R.: Size fractionation of iron, manganese
667 and aluminium in Antarctic fast ice reveals a lithogenic origin and low iron solubility, Mar. Chem., 161, 47–56,
668 doi:10.1016/j.marchem.2014.02.006, 2014.

669 Lee, J. M., Heller, M. I. and Lam, P. J.: Size distribution of particulate trace elements in the U.S. GEOTRACES
670 Eastern Pacific Zonal Transect (GP16), Mar. Chem., 201(September 2017), 108–123,
671 doi:10.1016/j.marchem.2017.09.006, 2017.

672 Lemaître, N., planquette, H., Planchon, F., Sarthou, G., Jacquet, S., Garcia-Ibanez, M. I., Gourain, A., Cheize,
673 M., Monin, L., Andre, L., Laha, P., Terryn, H., and Dehairs, F.: Particulate barium tracing significant mesopelagic
674 carbon remineralisation in the North Atlantic, Biogeosciences, doi:10.5194/bg-15-2289-2018, 2018a.

675 Lemaitre, N., Planchon, F., Planquette, H., Dehairs, F., Fonseca-Batista, D., Roukaerts, A., Deman, F., Tang, Y.,
676 Mariez, C., and Sarthou G.: High variability of export fluxes along the North Atlantic GEOTRACES section
677 GA01: Particulate organic carbon export deduced from the 234Th method, Biogeosciences, doi:10.5194/bg-2018-
678 190, 2018b.

679 Le Roy, E., Sanial, V., Charette, M.A., Van Beek, P., Lacan, F., Jacquet, S.H., Henderson, P.B., Souhaut, M.,
680 García-Ibáñez, M.I., Jeandel, C. and Pérez, F.: The 226Ra-Ba relationship in the North Atlantic during
681 GEOTRACES-GA01, Biogeosciences, doi:10.5194/bg-2017-478, 2018.

682 Marsay, C. M., Lam, P. J., Heller, M. I., Lee, J. M. and John, S. G.: Distribution and isotopic signature of ligand-
683 leachable particulate iron along the GEOTRACES GP16 East Pacific Zonal Transect, Mar. Chem., (November
684 2016), 1–14, doi:10.1016/j.marchem.2017.07.003, 2017.

685 Martin, J. H., Fitzwater, S. E., Michael Gordon, R., Hunter, C. N. and Tanner, S. J.: Iron, primary production and
686 carbon-nitrogen flux studies during the JGOFS North Atlantic bloom experiment, Deep. Res. Part II, 40(1–2),
687 115–134, doi:10.1016/0967-0645(93)90009-C, 1993.

688 McCave, I. N. and Hall, I. R.: Turbidity of waters over the Northwest Iberian continental margin, Prog. Oceanogr.,
689 52(2–4), 299–313, doi:10.1016/S0079-6611(02)00012-5, 2002.

690 Menzel Barraqueta, J.L., Schlosser, C., Planquette, H., Gourain, A., Cheize, M., Boutorh, J., Shelley, R., Pereira
691 Contreira, L., Gledhill, M., Hopwood, M.J. and Lherminier, P.: Aluminium in the North Atlantic Ocean and the
692 Labrador Sea (GEOTRACES GA01 section): roles of continental inputs and biogenic particle removal.
693 Biogeosciences, 1-28, doi: 10.5194/bg-2018-39, 2018.
694
695 Menzel Barraqueta, J.-L., Klar, J. K., Gledhill, M., Schlosser, C., Shelley, R., Planquette, H., Wenzel, B.,
696 Sarthou, G., and Achterberg, E. P.: Atmospheric aerosol deposition fluxes over the Atlantic Ocean: A
697 GEOTRACES case study, Biogeosciences Discuss., https://doi.org/10.5194/bg-2018-209, in review, 2018b.

698 Milne, A., Schlosser, C., Wake, B. D., Achterberg, E. P., Chance, R., Baker, A. R., Forryan, A. and Lohan, M.
699 C.: Particulate phases are key in controlling dissolved iron concentrations in the (sub)tropical North Atlantic,
700 Geophys. Res. Lett., 44(5), 2377–2387, doi:10.1002/2016GL072314, 2017.

701 Nuester, J., Shema, S., Vermont, A., Fields, D. M. and Twining, B. S.: The regeneration of highly bioavailable
702 iron by meso- and microzooplankton, Limnol Oceanogr, 59(4), 1399–1409, doi:10.4319/lo.2014.59.4.1399, 2014.

Oelkers, E. H., Jones, M. T., Pearce, C. R., Jeandel, C., Eiriksdottir, E. S. and Gislason, S. R.: Riverine particulate material dissolution in seawater and its implications for the global cycles of the elements, Geosci., 344(11–12), 646–651, doi:10.1016/j.crte.2012.08.005, 2012.

Ohnemus, D. C. and Lam, P. J.: Cycling of lithogenic marine particles in the US GEOTRACES North Atlantic transect, Deep. Res. Part II Top. Stud. Oceanogr., 116, 283–302, doi:10.1016/j.dsr2.2014.11.019, 2015.

Peers, G. and Price, N. M.: A role for manganese in superoxide dismutases and growth of iron-deficient diatoms, Limnol. Oceanogr., 49(5), 1774–1783, doi:10.4319/lo.2004.49.5.1774, 2004.

Planquette, H. and Sherrell, R. M.: Sampling for particulate trace element determination using water sampling bottles: Methodology and comparison to in situ pumps, Limnol. Oceanogr. Methods, 10(5), 367–388, doi:10.4319/lom.2012.10.367, 2012.

Planquette, H., Fones, G. R., Statham, P. J. and Morris, P. J.: Origin of iron and aluminium in large particles (> 53 μm) in the Crozet region, Southern Ocean, Mar. Chem., 115(1–2), 31–42, doi:10.1016/j.marchem.2009.06.002, 2009.

Planquette, H., Sanders, R. R., Statham, P. J., Morris, P. J. and Fones, G. R.: Fluxes of particulate iron from the upper ocean around the Crozet Islands: A naturally iron-fertilized environment in the Southern Ocean, Global Biogeochem. Cycles, 25(2), doi:10.1029/2010GB003789, 2011.

Planquette, H., Sherrell, R. M., Stammerjohn, S. and Field, M. P.: Particulate iron delivery to the water column of the Amundsen Sea, Antarctica, Mar. Chem., 153, 15–30, doi:10.1016/j.marchem.2013.04.006, 2013.

Radic, A., Lacan, F. and Murray, J. W.: Iron isotopes in the seawater of the equatorial Pacific Ocean: New constraints for the oceanic iron cycle, Earth Planet. Sci. Lett., 306(1–2), 1–10, doi:10.1016/j.epsl.2011.03.015, 2011.

Raiswell, R., Benning, L. G., Tranter, M. and Tulaczyk, S.: Bioavailable iron in the Southern Ocean: The significance of the iceberg conveyor belt, Geochem. Trans., 9(1), 7, doi:10.1186/1467-4866-9-7, 2008.

Rijkenberg, M. J. A., Middag, R., Laan, P., Gerringa, L. J. A., Van Aken, H. M., Schoemann, V., De Jong, J. T. M. and De Baar, H. J. W.: The distribution of dissolved iron in the West Atlantic Ocean, PLoS One, 9(6), 1–14, doi:10.1371/journal.pone.0101323, 2014.

Sanders, R., Henson, S. A., Koski, M., De La Rocha, C. L., Painter, S. C., Poulton, A. J., Riley, J., Salihoglu, B., Visser, A., Yool, A., Bellerby, R. and Martin, A. P.: The Biological Carbon Pump in the North Atlantic, Prog. Oceanogr., 129(PB), 200–218, doi:10.1016/j.pocean.2014.05.005, 2014.

Sarthou, G., Lherminier, and the GEOVIDE team: Introduction to the French GEOTRACES North Atlantic Transect (GA01): GEOVIDE cruise, Biogeosciences, 15, 7097-7109, https://doi.org/10.5194/bg-15-7097-2018, 2018.

Sarthou, G., Vincent, D., Christaki, U., Obernosterer, I., Timmermans, K. R. and Brussaard, C. P. D.: The fate of biogenic iron during a phytoplankton bloom induced by natural fertilisation: Impact of copepod grazing, Deep. Res. Part II Top. Stud. Oceanogr., 55(5–7), 734–751, doi:10.1016/j.dsr2.2007.12.033, 2008.

Schlosser, C., Schmidt, K., Aquilina, A., Homoky, W. B., Castrillejo, M., Mills, R. A., Patey, M. D., Fielding, S., Atkinson, A. and Achterberg, E. P.: Mechanisms of dissolved and labile particulate iron supply to shelf waters and phytoplankton blooms off South Georgia, Southern Ocean, Biogeosciences, 15, 4973–4993, doi: 10.5194/bg-15-4973-2018, 2018.

Shelley, R. U., Landing, W. M., Ussher, S. J., Planquett, H. and Sarthou, G.: Characterisation of aerosol provenance from the fractional solubility of Fe (Al, Ti, Mn, Co, Ni, Cu, Zn , Cd and Pb) in North Atlantic aerosols (GEOTRACES GA01 and GA03), Biogeosciences, 15, 2271–2288, doi: 10.5194/bg-15-2271-2018, 2018

Shelley, R. U., Landing, W. M., Ussher, S. J., Planquette, H. and Sarthou, G.: Regional trends in the fractional solubility of Fe and other metals from North Atlantic aerosols (GEOTRACES cruises GA01 and GA03) following a two-stage leach, Biogeosciences, 155194(1), 2271–2288, doi:10.5194/bg-15-2271-2018, 2018.

Sherrell, R. M., Field, P. M. and Gao, Y.: Temporal variability of suspended mass and composition in the Northeast Pacific water column: Relationships to sinking flux and lateral advection, Deep. Res. Part II Top. Stud. Oceanogr., 45(4–5), 733–761, doi:10.1016/S0967-0645(97)00100-8, 1998.

Spinrad, R. W.,Zaneveld, J. R. and Kitchen, J.C.: A Study of the Optical Characteristics of the Suspended Particles Benthic N epheloid Layer of the Scotian Rise, J. Geophys. Res., 88, 7641–7645, doi:0148-0227/83/003C, 1983.

Statham, P. J., Skidmore, M. and Tranter, M.: Inputs of glacially derived dissolved and colloidal iron to the coastal ocean and implications for primary productivity, Global Biogeochem. Cycles, 22(3), 1–11, doi:10.1029/2007GB003106, 2008.

Straneo, F., Pickart, R. S. and Lavender, K.: Spreading of Labrador sea water: An advective-diffusive study based on Lagrangian data, Deep. Res. Part I Oceanogr. Res. Pap., 50(6), 701–719, doi:10.1016/S0967-0637(03)00057-8, 2003.

Sunda, W. G. and Huntsman, S. A.: Effect of Competitive Interactions Between Manganese and Copper on Cellular Manganese and Growth in Estuarine and Oceanic Species of the Diatom Thalassiosira, Limnol. Oceanogr., 28(5), 924–934, doi:10.4319/lo.1983.28.5.0924, 1983.

Tagliabue, A., Bopp, L., Dutay, J. C., Bowie, A. R., Chever, F., Jean-Baptiste, P., Bucciarelli, E., Lannuzel, D., Remenyi, T., Sarthou, G., Aumont, O., Gehlen, M. and Jeandel, C.: Hydrothermal contribution to the oceanic dissolved iron inventory, Nat. Geosci., 3(4), 252–256, doi:10.1038/ngeo818, 2010.

Tagliabue, A., Bowie, A. R., Boyd, P. W., Buck, K. N., Johnson, K. S. and Saito, M. A.: The integral role of iron in ocean biogeochemistry, Nature, 543(7643), 51–59, doi:10.1038/nature21058, 2017.

767 Taylor, S. and McLennan, S.: The geochemical evolution of the continental crust, Rev. Geophys., 33(2), 241–
768 265, doi:10.1029/95RG00262, 1995.

769 Tebo, B. M. and Emerson, S. R.: Effect of Oxygen Tension Manganese (II) Concentration and Temperature on
770 the Microbially Catalyzed Manganese-Ii Oxidation Rate in a Marine Fjord, Appl. Environ. Microbiol., 50(5),
771 1268–1273, 1985.

772 Tebo, B. M., Nealson, K. H., Emerson, S. and Jacobs, L.: Microbial mediation of Mn(II) and Co(II) precipitation
773 at the o2/H2S interfaces in two anoxic fjords, 29(6), 1247–1258, 1984.

774 Tonnard, M., Planquette, H., Bowie, A. R., van der Merwe, P., Gallinari, M., Desprez de Gésincourt, F., Germain,
775 Y., Gourain, A., Benetti, M., Reverdin, G., Tréguer, P., Boutorh, J., Cheize, M., Menzel Barraqueta, J.L., Pereira-
776 Contreira, L., Shelley, R., Lherminier, P., and Sarthou, G.: Dissolved iron in the North Atlantic Ocean and
777 Labrador Sea along the GEOVIDE section (GEOTRACES section GA01), Biogeosciences Discuss.,
778 https://doi.org/10.5194/bg-2018-147, 2018

779 Trefry, J. H., Trocine, R. P., Klinkhammer, G. P. and Rona, P. A.: Iron and copper enrichment of suspended
780 particles in dispersed hydrothermal plumes along the mid-Atlantic Ridge, Geophys. Res. Lett., 12(8), 506–509,
781 doi:10.1029/GL012i008p00506, 1985.

782 Ussher, S. J., Achterberg, E. P. and Worsfold, P. J.: Marine biogeochemistry of iron, Environ. Chem., 1(2), 67–
783 80, doi:10.1071/EN04053, 2004.

784 Ussher, S. J., Worsfold, P. J., Achterberg, E. P., Laës, A., Blain, S., Laan, P., de Baar, H. J. W.: Distribution and
785 redox speciation of dissolved iron on the European continental margin, Limnol. Oceanogr., 52(6), 2530–2539,
786 doi:10.4319/lo.2007.52.6.2530, 2007.

787 Van der Merwe, P., Lannuzel, D., Bowie, A. R., Mancuso Nichols, C. A. and Meiners, K. M.: Iron fractionation
788 in pack and fast ice in East Antarctica: Temporal decoupling between the release of dissolved and particulate iron
789 during spring melt, Deep. Res. Part II Top. Stud. Oceanogr., 58(9–10), 1222–1236,
790 doi:10.1016/j.dsr2.2010.10.036, 2011a.

791 Van Der Merwe, P., Lannuzel, D., Bowie, A. R. and Meiners, K. M.: High temporal resolution observations of
792 spring fast ice melt and seawater iron enrichment in East Antarctica, J. Geophys. Res. Biogeosciences, 116(3), 1–
793 18, doi:10.1029/2010JG001628, 2011b.

794 Weinstein, S. E. and Moran, S. B.: Distribution of size-fractionated particulate trace metals collected by bottles
795 and in-situ pumps in the Gulf of Maine-Scotian Shelf and Labrador Sea, Mar. Chem., 87(3–4), 121–135,
796 doi:10.1016/j.marchem.2004.02.004, 2004.

797 Yashayaev, I.: Hydrographic changes in the Labrador Sea, 1960-2005, Prog. Oceanogr., 73(3–4), 242–276,
798 doi:10.1016/j.pocean.2007.04.015, 2007.

Yashayaev, I. and Loder, J. W.: Enhanced production of Labrador Sea Water in 2008, Geophys. Res. Lett., 36(1), doi:10.1029/2008GL036162, 2009.

Zunino, P., Lherminier, P., Mercier, H., Daniault, N., García-Ibáñez, M. I., and Pérez, F. F.: The GEOVIDE cruise in May–June 2014 reveals an intense Meridional Overturning Circulation over a cold and fresh subpolar North Atlantic. Biogeosciences, 14(23), 5323, 2017.

Figure 1: Map of stations where suspended particle samples were collected with GO-FLO bottles during the GEOVIDE cruise (GA01) in the North Atlantic Ocean. Biogeochemical provinces are indicated by red squares, IM: Iberian Margin, IAP: Iberian Abyssal Plain, WEB: Western European Basin, IcB: Iceland Basin, RR: Reykjanes Ridge, IrB: Irminger Basin, GS: Greenland Shelf, LB: Labrador Basin, NS: Newfoundland Shelf. This figure was generated using Ocean Data View (Schlitzer, R., Ocean Data View, odv.awi.de, 2017).

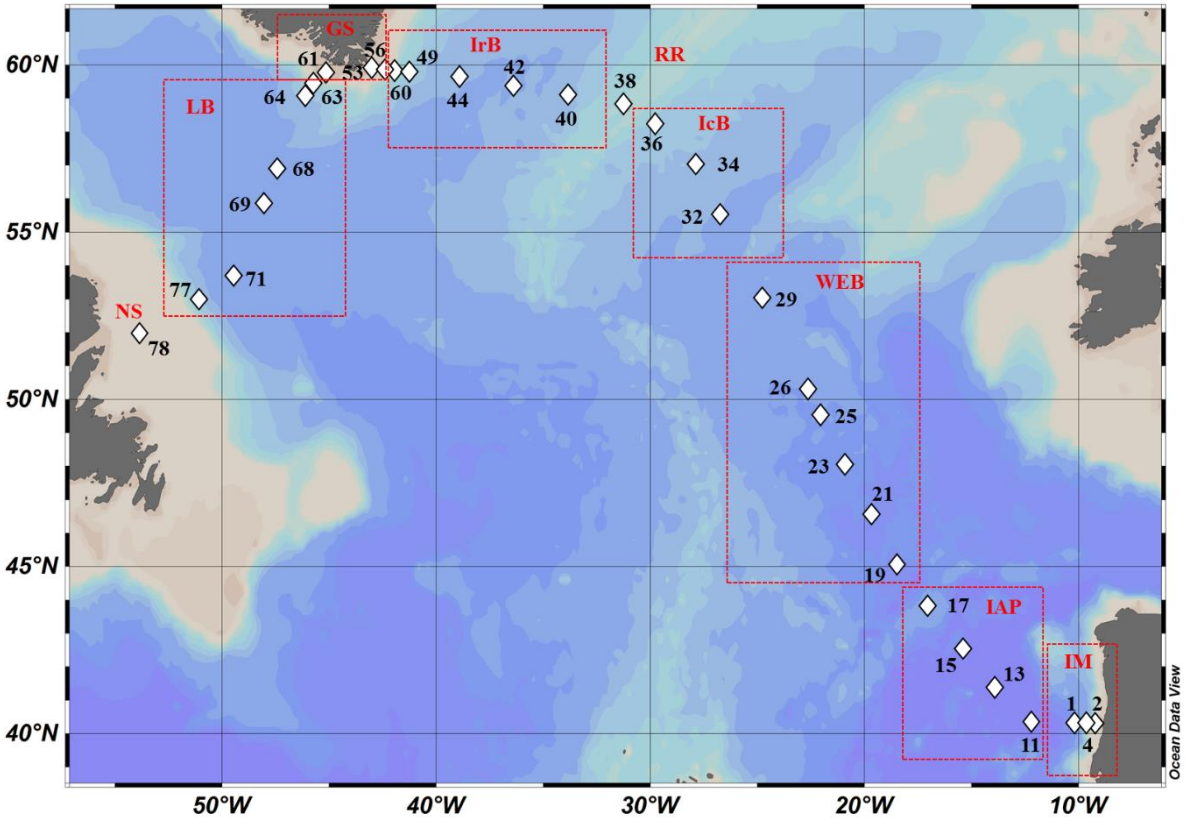

Figure 2: Salinity section during the GEOVIDE cruise with water masses indicated in black italic font. A salinity contour of 35.8 psu have been applied to identify the Mediterranean Water (MW) to the east. From right to left; North East Atlantic Deep Water (NEADW); North Atlantic Central Water (NACW); Labrador Sea Water (LSW); Sub-Arctic Intermediate Water (SAIW); Iceland-Scotland Overflow Water (ISOW); Iceland Sub-Polar Mode Water (IcSPMW); Denmark Strait Overflow Water (DSOW); Irminger Sub-Polar Mode Water (IrSPMW). Station locations are indicated by the numbers above the section and biogeochemical provinces are indicated in blue font above station numbers. This figure was generated using Ocean Data View (Schlitzer, R., Ocean Data View, odv.awi.de, 2017).

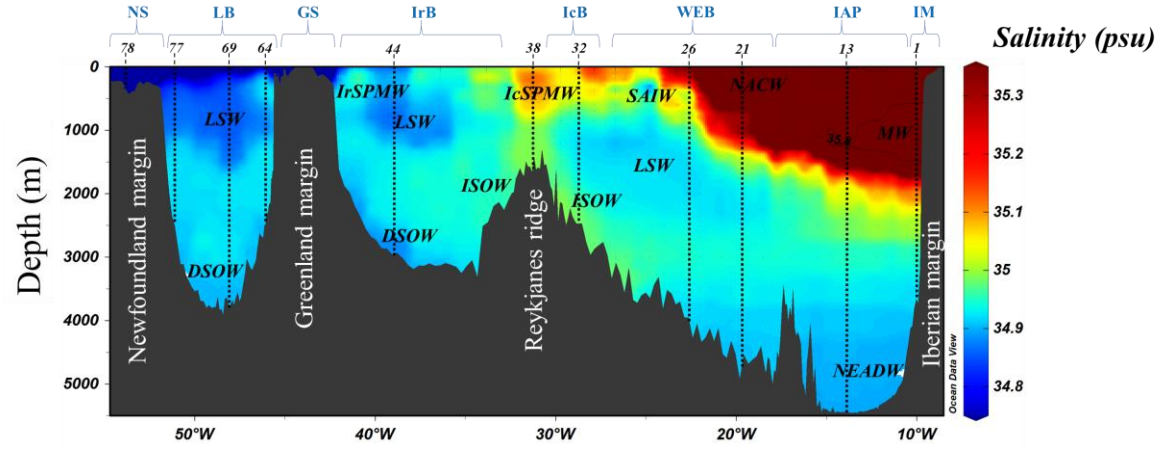

Figure 3: Left panel: Distribution of total particulate (a) iron (PFe), (b) aluminium (PAl), (c) manganese (PMn) and (d) phosphorus (PP) concentrations (nmol L^{-1}) in the first 250 m and the entire water column along the GEOVIDE section in the North Atlantic Ocean. Right panel: Contribution of the small size fraction (0.45-5 µm) expressed as a percentage (%) of the total concentration of (e) PFe, (f) PAl, (g) PMn and (h) PP. Station IDs and biogeochemical regions are indicated on top of sections a and e. This figure was generated using Ocean Data View (Schlitzer, R., Ocean Data View, odv.awi.de, 2017).

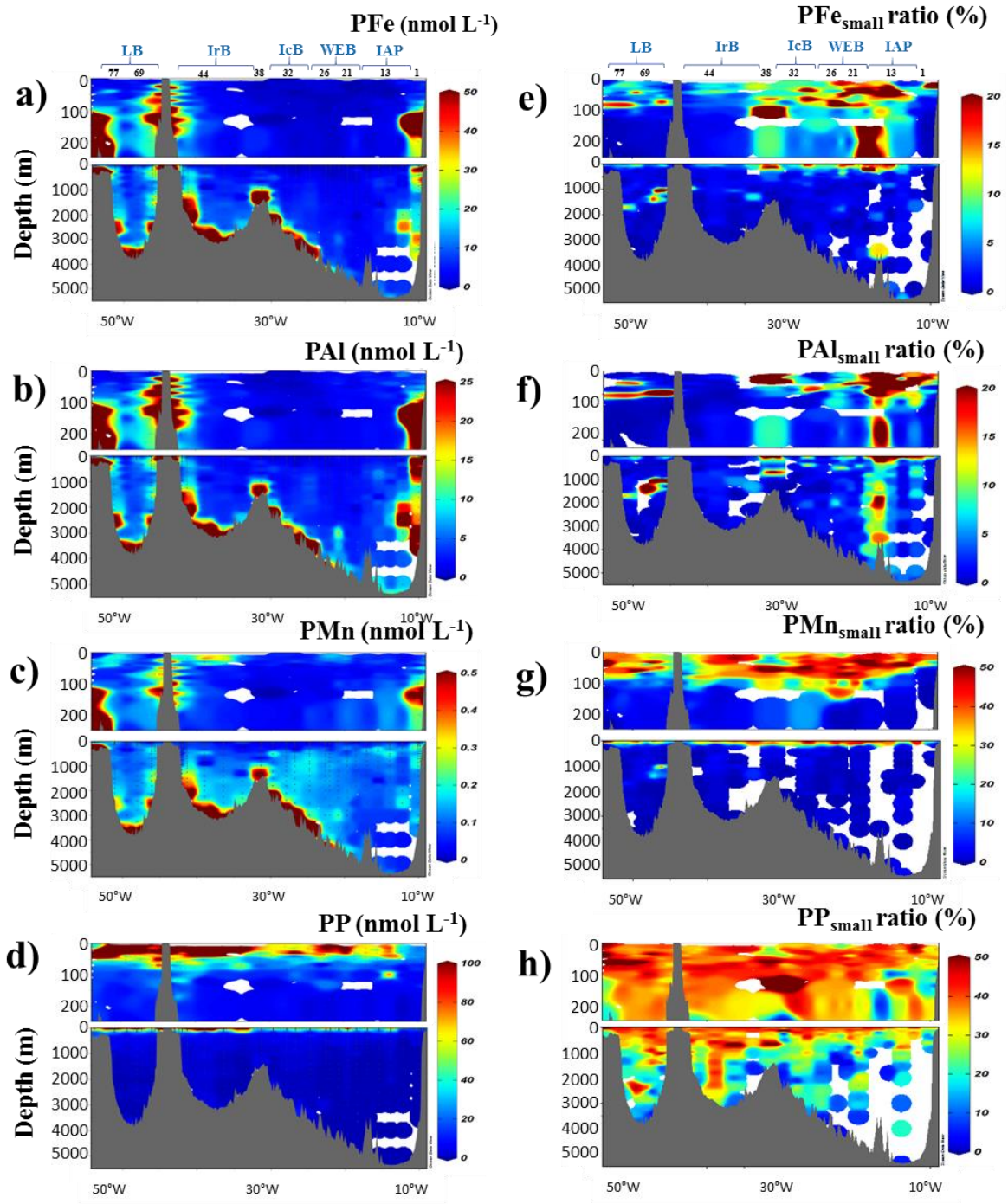

Figure 4: Section of derived contributions of sedimentary inputs along the GA01 section with (a) beam transmissometry (%) and (b) manganese bulk sediment proxy (%) based on Eq (3). Station IDs and biogeochemical region are indicated above section (a) in black numbers and blue letters, respectively. This figure was generated using Ocean Data View (Schlitzer, R., Ocean Data View, odv.awi.de, 2017).

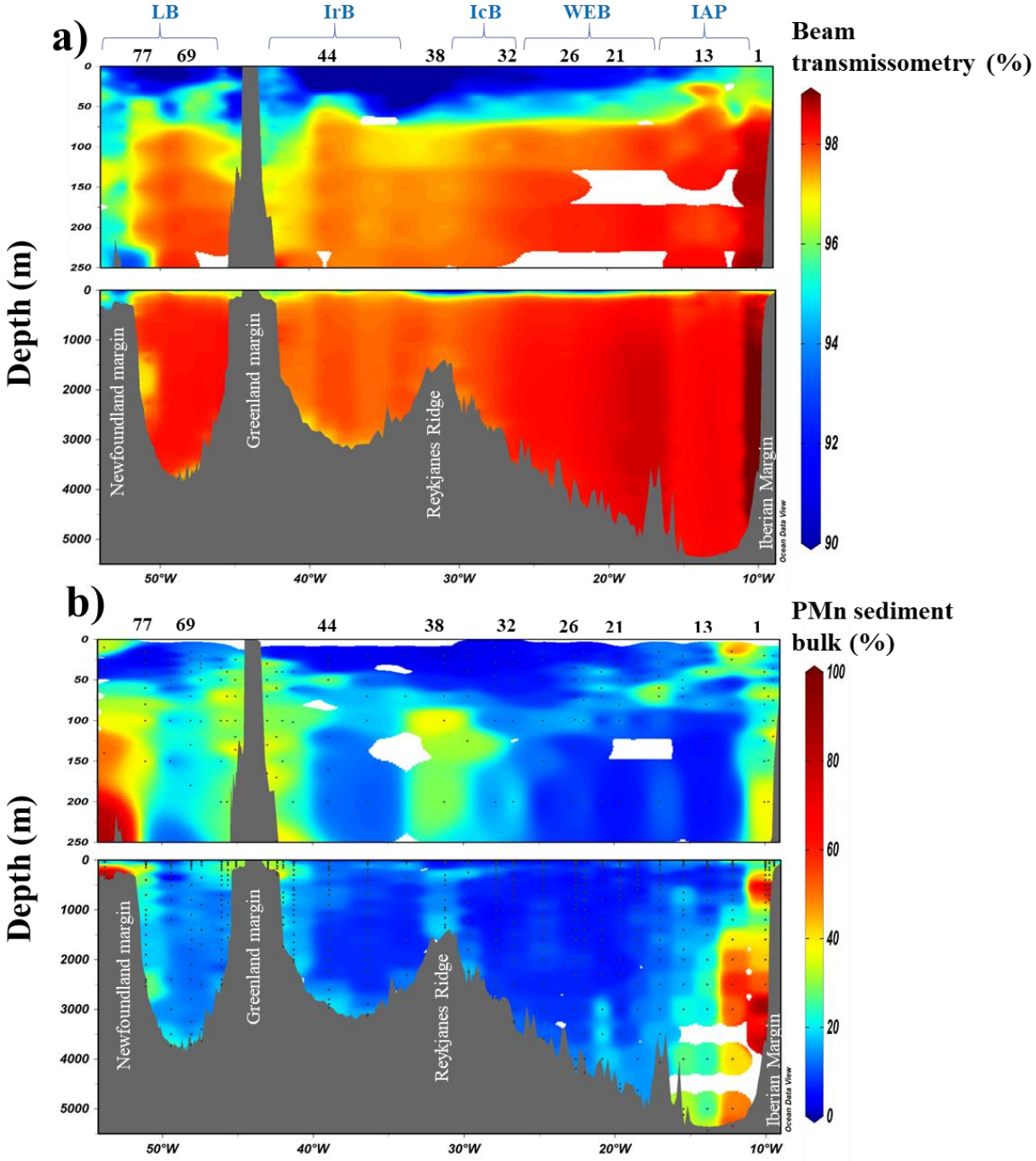

Figure 5: Factor fingerprint of the positive matrix factorisation conducted on 445 particles samples collected along the GA01 section. The four main factors influencing the particulate trace element variance are represented in a stacked bar chart of the percentage of variance explained per element. Factor 1 is dominated by the lithogenic elements, e.g. Th, Al, Ti and Fe. Factor 2 is associated with Pb and Mn variances. Biogenic barite formation mainly influences factor 3. Factor 4 is dominated by biogenic elements, e.g. P, Co, Cu and Zn.

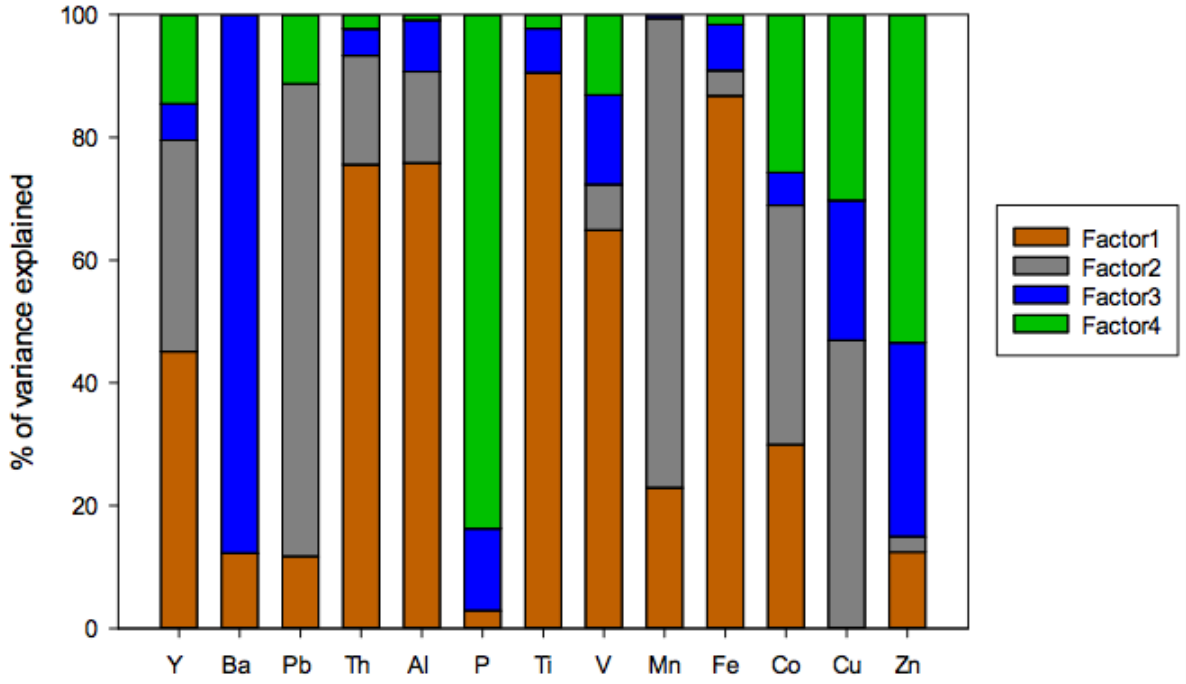

Figure 6: a) Section of the PFe to PAl molar ratio (mol mol^{-1}) during the GEOVIDE cruise (GA01) and (b) contribution (%) of lithogenic particulate iron (PFe_{litho}) based on Eq. (1). Station IDs and biogeochemical provinces are indicated above each section in black numbers and blue letters, respectively. This figure was generated using Ocean Data View (Schlitzer, R., Ocean Data View, odv.awi.de, 2017).

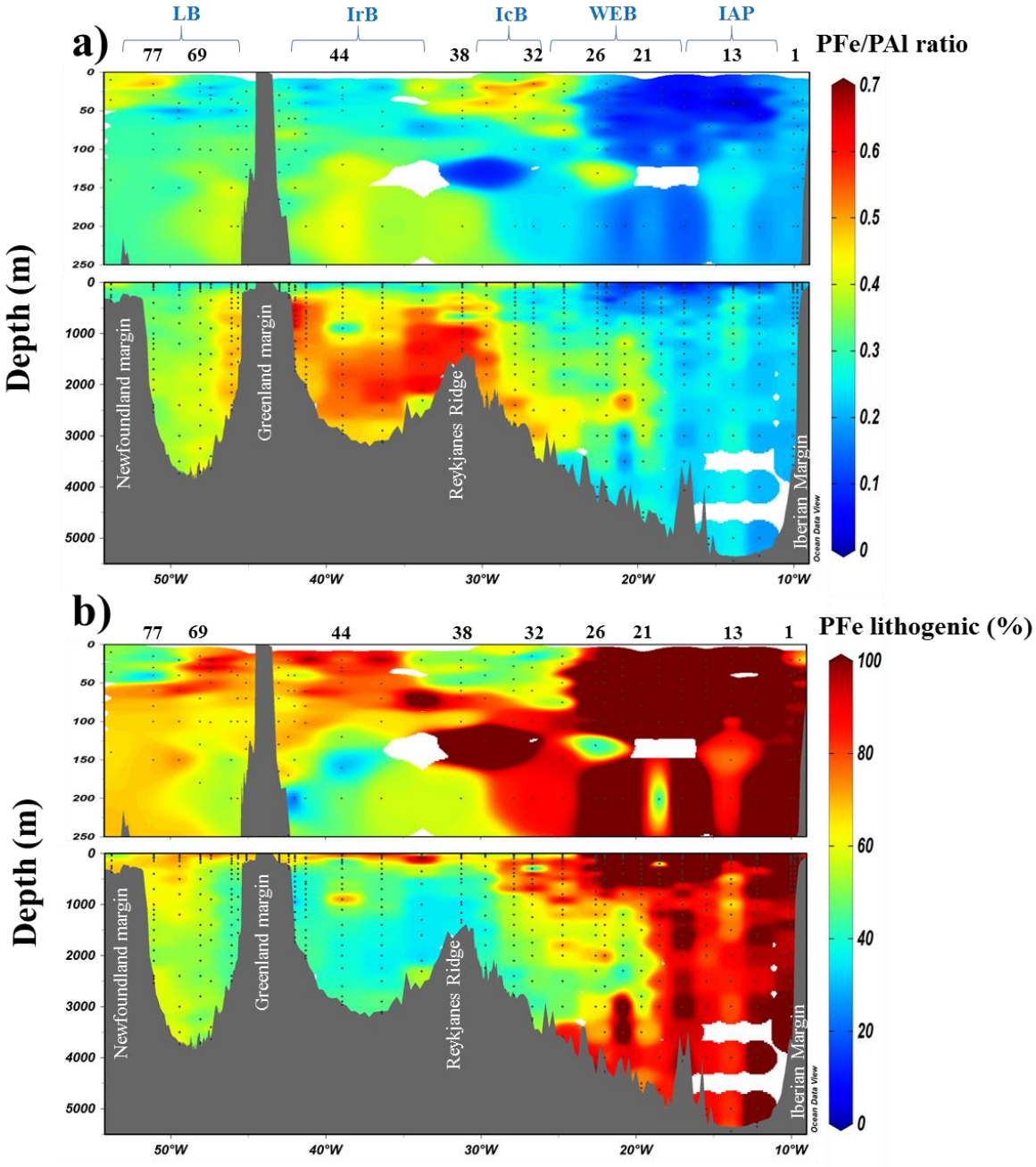

Figure 7: Box and whisker diagram of PFe/PAl molar ratio in nine water masses sampled along the GA01 section in the North Atlantic Ocean. Water masses are defined in section 3.1 and in Figure 2. The PFe/PAl median values for each water masses with the biogeochemical provinces in subscript were as follows: LSW_{LB} = 0.37; LSW_{IrB} = 0.44; LSW_{WEB} = 0.36; $ISOW_{IcB}$ = 0.48; $ISOW_{IrB}$ = 0.58; $DSOW_{LB}$ = 0.42; $DSOW_{IrB}$ = 0.47; $NEADW_{IAP}$ = 0.23; MW = 0.22 mol mol^{-1}. The difference in PFe/PAl between water masses is statistically significant (Kruskal-Wallis test; p = < 0.001 excluding water masses for which we had less than 5 data points for PFe/PAl). Noted that the UCC PFe/PAl ratio reported from Taylor and McLennan, (1995) is 0.21 mol mol^{-1}.

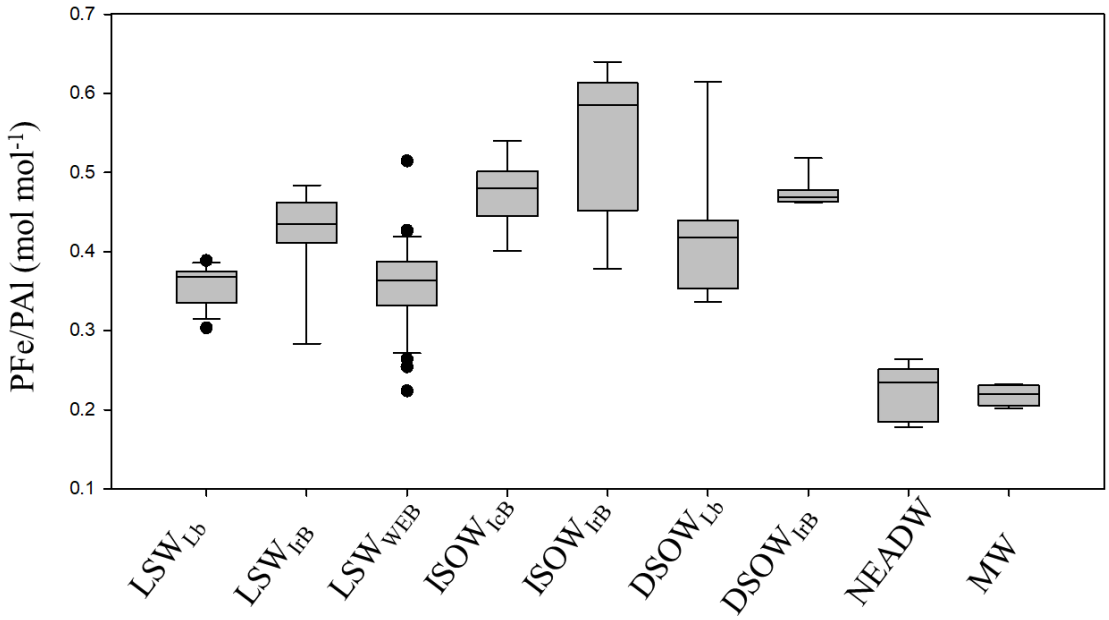

966 **Figure 8: Vertical profiles of (a) PFe (nmol L^{-1}), (b) lithogenic proportion of particulate iron (PFe_{litho}, %) and (c)**
967 **sedimentary proportion of particulate manganese (PMn sediment, %) at the Iberian, East-West Greenland and**
968 **Newfoundland margins.**

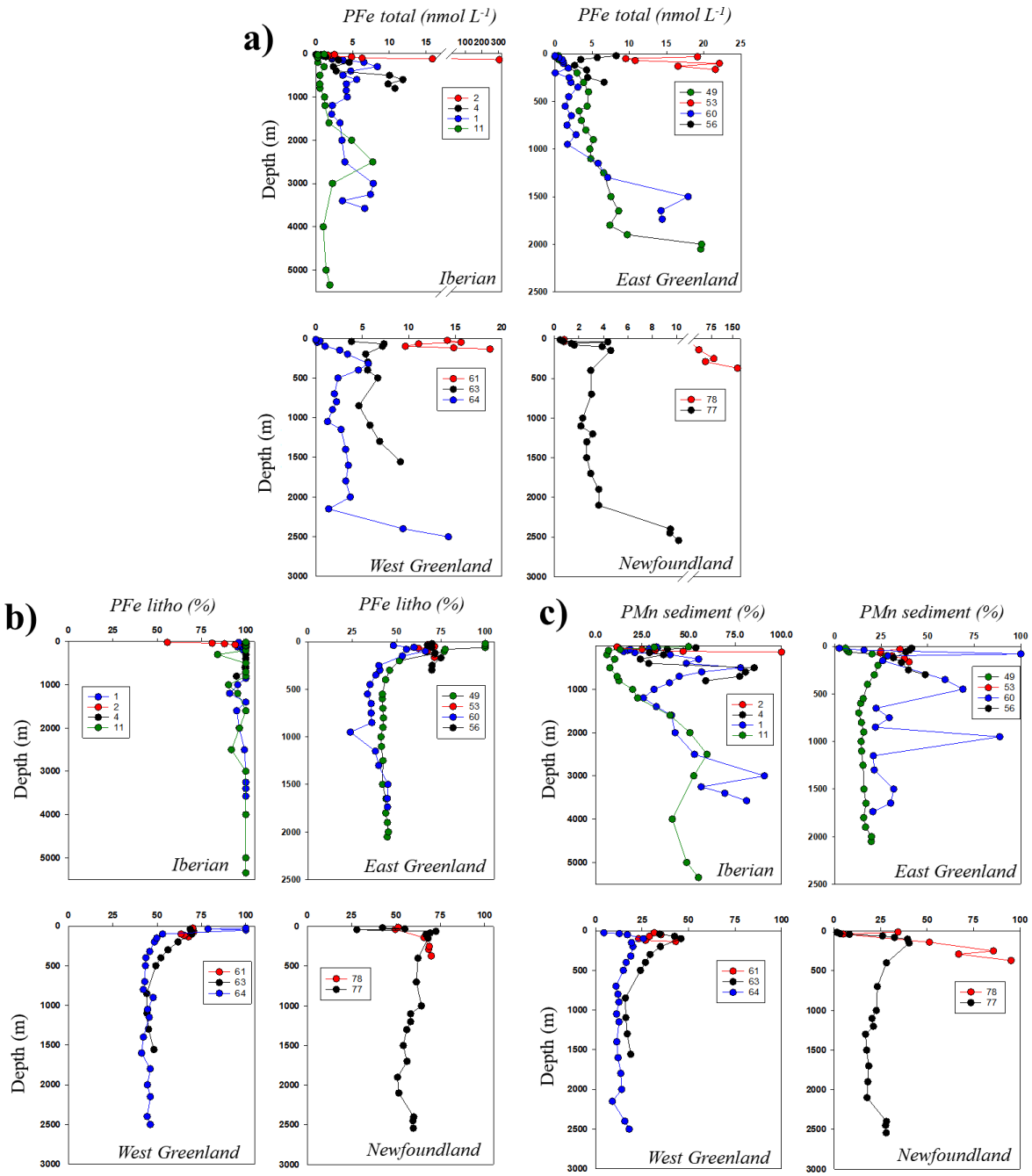

969

970

971

972

973

974

975

Figure 9: Scatter of the PFe/PAl ratio at the Iberian (red dots), East Greenland (black dots), West Greenland (green dots) and Newfoundland margins (blue dots). Dashed line indicate the UCC PFe/PAl ratio (Taylor and McLennan, 1995).

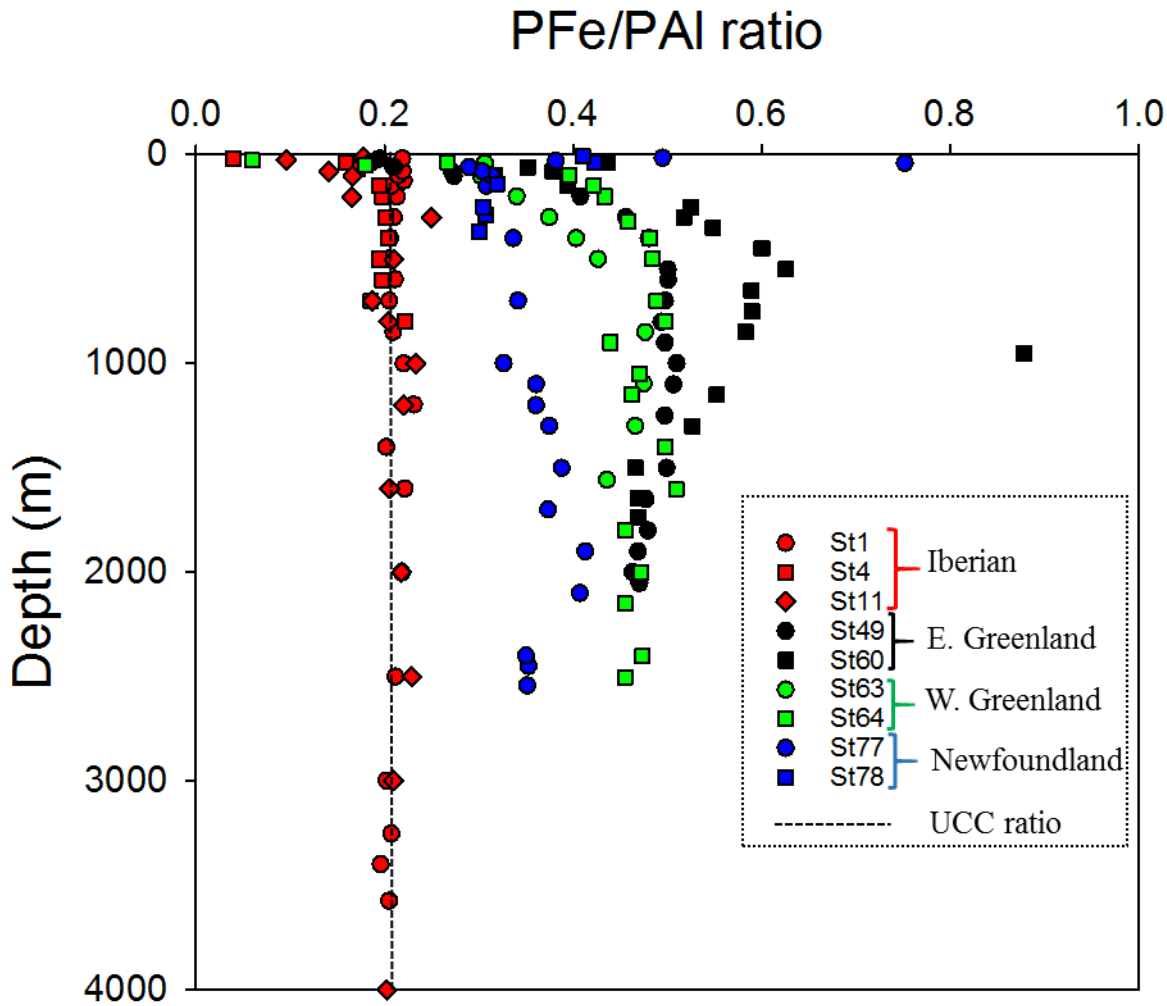

Figure 10: Benthic Nepheloid Layers (BNLs) encountered along the GA01 section and observed through a) PFe total; b) PFe/PAl ratio and c) beam transmissometry (%) as a function of depth above the seafloor (m) at selected stations where a decrease in transmissometry was recorded in the West European (red dots), the Iceland (green dots), the Irminger (blue dots) and the Labrador Basins. Noted that the UCC PFe/PAl ratio reported fromTaylor and McLennan, (1995) is 0.21 mol mol^{-1}.

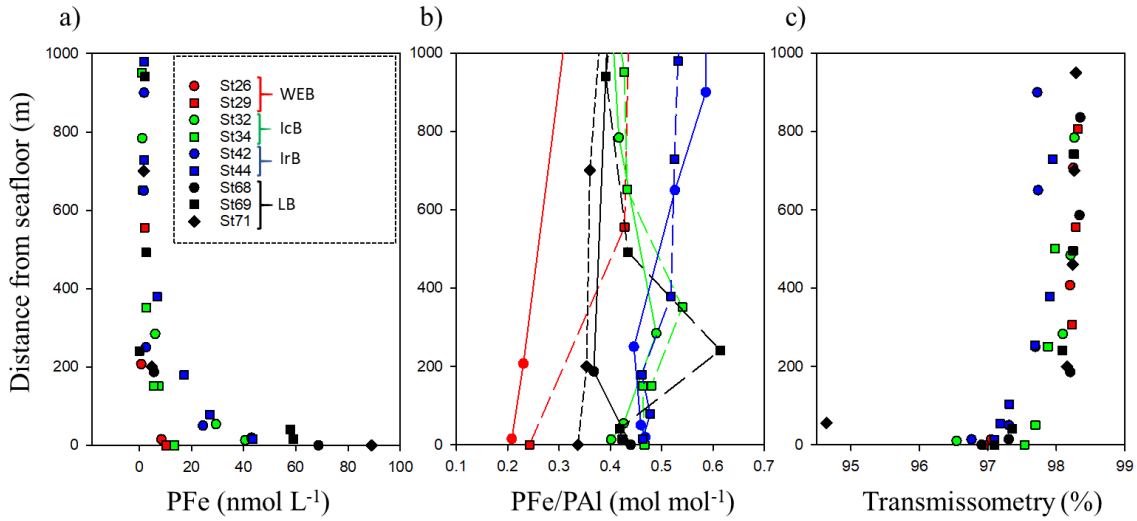

		Fe	Al	P	Mn
Blank (nmol L^{-1})	5µm filter	0.072	0.100	0.511	0.003
	0.45µm filter	0.132	0.164	1.454	0.005
Limit of detection (nmol L^{-1})	5µm filter	0.011	0.030	0.365	0.001
	0.45µm filter	0.026	0.046	1.190	0.001
Recovery CRM (%)	BCR-414 (n=10)	88 ± 7			94 ± 7
	MESS-4 (n=5)	98 ± 14	97 ± 14	80 ± 30	110 ± 18
	PACS-3 (n=8)	101 ± 9	99 ± 14	91 ± 34	112 ± 11

Table 1: Blank and limit of detection (nmol L^{-1}) of the two filters and certified reference material (CRM) recoveries during GEOVIDE suspended particle digestions.

Location	Depth range	PFe	PAl	PMn	PP	Fraction	Author	Year
N. Atlantic (>40°N)	All	bdl-304	bdl-1544	bdl-3.5	bdl-402	>0.45µm	This study	
Labrador Sea	0-250	0.1-1.2	0.1-1.5			>53 µm	Weinstein et al.	2004
Labrador Sea	0-250	2.5	3.6	0.05		0.4– 10um	Weinstein et al.	2004
N. Atlantic (25-60°N)	Upper 1000m	0.29-1.71	0.2-19.7			0.4um	Barrett et al.	2012
N. Atlantic	All	0-938	0-3600			0.8–51 µm	Ohnemus et al.	2015
Gulf of Maine	0-300	34.8	109			>0.4 µm	Weinstein et al.	2004
Eastern tropical N.A.	0-200		0.59-17.7			>0.2 µm	Dammshauser et al.	2013
Eastern tropical N.A.	0-600	ND-12				1–51 um	Lam et al.	2012
Sub-tropical N.A.	All	ND-140	ND-800			>0.45µm	Milne et al.	2017
Meridional Atlantic	0-200		0.35-16.1			>0.2 µm	Dammshauser et al.	2013
Northeast Pacific	0-3557		0.0-54.2			1-53um	Sherrell et al.	1998
Eastern tropical S.Pacific	All	bdl-159	bdl-162	bdl-8.7	bdl-983	>0.8 µm	Lee et al.	2017
South Georgia Shelf	All	0.87-267	0.6-195	0.01-3.85		>1 µm	Schlosser et al.	2017
Southern Ocean	30-340	0.15–13.2	0.11–25.5			>53 µm	Planquette et al.	2009
East Antarctic	Surface		0.02-10.67	0.01-0.14		>0.2 µm	Lannuzel et al.	2011
East Antarctic	Fast ice	43-10385	121-31372	1-307		>0.2 µm	Lannuzel et al.	2014
Ross Sea	All	0.68-57.3	ND-185	ND-1.4	5.4-404	>0.4 µm	Marsay et al.	2017

Table 2: Concentration (in nmol L^{-1}) of particulate trace elements (PFe, Pal, PMn and PP) in suspended particles collected in diverse regions of the world's ocean. Bdl: below detection limit, ND: non-determined.